

AD-A240 392



2

PL-TR-91-2159

RADIATION BELT DYNAMIC AND QUASI-STATIC
MODELING BASED ON CRRES DATA

Y. T. Chiu
M. A. Rinaldi
W. E. Francis
R. M. Robinson
R. W. Nightingale

Lockheed Palo Alto Research Laboratory
Space Sciences Laboratory
3251 Hanover Street
Palo Alto, CA 94304-1191

17 June 1991

DTIC
ELECTE
SEP 12 1991
S B D

Scientific Report No. 1

APPROVED FOR PUBLIC RELEASE; DISTRIBUTION UNLIMITED



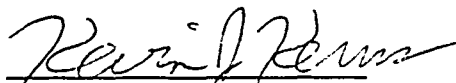
PHILLIPS LABORATORY
AIR FORCE SYSTEMS COMMAND
HANSCOM AIR FORCE BASE, MASSACHUSETTS 01731-5000

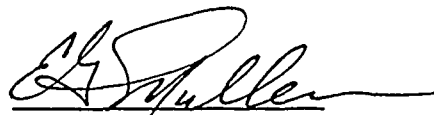
91 9 9 088

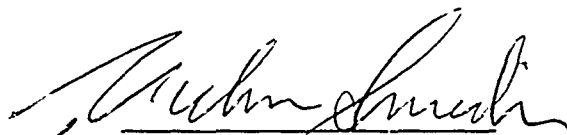
91-10182



"This technical report has been reviewed and is approved for publication"


KEVIN KERNS, Lt, USAF
Contract Manager


E. G. MULLEN
Branch Chief


for RITA C. SAGALYN
Division Director

This document has been reviewed by the ESD Public Affairs Office (PA) and is releasable to the National Technical Information Service (NTIS).

Qualified requestors may obtain additional copies from the Defense Technical Information Center. All others should apply to the National Technical Information Service.

If your address has changed, or if you wish to be removed from the mailing list, or if the addressee is no longer employed by your organization, please notify GL/IMA, Hanscom AFB, MA 01731. This will assist us in maintaining a current mailing list.

Do not return copies of this report unless contractual obligations or notices on a specific document requires that it be returned.

REPORT DOCUMENTATION PAGE			Form Approved OMB No 0704-0188	
<small>Public reporting burden for this collection of information is estimated to average 1 hour per response, including the time for reviewing instructions, searching existing data sources, gathering and maintaining the data needed, and completing and reviewing the collection of information. Send comments regarding this burden estimate or any other aspect of this collection of information, including suggestions for reducing this burden, to Washington Headquarters Services, Directorate for Information Operations and Reports, 1215 Jefferson Davis Highway, Suite 1204, Arlington, VA 22202-4302, and to the Office of Management and Budget, Paperwork Reduction Project (0704-0188), Washington, DC 20503.</small>				
1. AGENCY USE ONLY (Leave blank)	2. REPORT DATE 17 June 1991	3. REPORT TYPE AND DATES COVERED Scientific Report No. 1		
4. TITLE AND SUBTITLE Radiation Belt Dynamic and Quasi-Static Modeling Based on CRRES Data		5. FUNDING NUMBERS PE 62101F PR 7601 TA 22 WU LA Contract F19628-90-C-0097		
6. AUTHOR(S) Y. T. Chiu M. A. Rinaldi W. E. Francis R. M. Robinson R. W. Nightingale				
7. PERFORMING ORGANIZATION NAME(S) AND ADDRESS(ES) Lockheed Palo Alto Research Laboratory Space Sciences Laboratory 3251 Hanover Street Palo Alto, CA 94304-1191		8. PERFORMING ORGANIZATION REPORT NUMBER		
9. SPONSORING / MONITORING AGENCY NAME(S) AND ADDRESS(ES) Phillips Laboratory Hanscom AFB, MA 01731-5000 Contract Manager: Kevin Kerns, Lt, USAF/PHP		10. SPONSORING / MONITORING AGENCY REPORT NUMBER PL-TR-91-2159		
11. SUPPLEMENTARY NOTES				
12a. DISTRIBUTION / AVAILABILITY STATEMENT APPROVED FOR PUBLIC RELEASE; DISTRIBUTION UNLIMITED		12b. DISTRIBUTION CODE		
13. ABSTRACT (Maximum 200 words) This report summarizes achievements made in the first year of the subject contract. New results on modeling the outer magnetosphere have been derived in order to provide an interpretation of CRRES radiation belt data. New features of the outer radiation belt dynamic response to geomagnetic storms are characterized using CRRES data. Detailed analysis of a benchmark event is presented.				
14. SUBJECT TERMS Radiation belts Geomagnetic storms Radiation dose		15. NUMBER OF PAGES 56		
		16. PRICE CODE		
17. SECURITY CLASSIFICATION OF REPORT Unclassified	18. SECURITY CLASSIFICATION OF THIS PAGE Unclassified	19. SECURITY CLASSIFICATION OF ABSTRACT Unclassified	20. LIMITATION OF ABSTRACT SAR	

Contents

1.	Introduction	1
2.	Outer Magnetosphere Modeling	2
3.	Diffusion Modeling	3
4.	Particle Encounters with Outer Magnetosphere Structures	4
5.	Test Case: Storm of August 1990	7
6.	Future Work	11
7.	Publications	12

Illustrations/Figures

1.	Magnetosphere in Paraboloidal Co-ordinates	13
2.	Open Outer Magnetosphere without Tail Structure	14
3.	Source-surface Model Outer Magnetosphere with Earthward IMF	15
4.	Source-surface Model Outer Magnetosphere with Northward IMF	16
5.	Pitch-angle Amplitudes for 800 KeV Electrons at Orbit 77	17
6.	Pitch-angle Amplitudes for 400 KeV Electrons at Orbit 82	18
7.	Magnetopause Stand-off Distance and IMF for Day 238, 1990	19
8.	CRRES Orbit and Modelled Magnetopause on Day 238, 1990	20
9.	ONR-307 SEP Electron Flux Spectrographs on Orbits 75, 77 and 79	21
10.	Pitch-angle Distributions for 400 KeV Electrons at L=5.4	22
11.	Pitch-angle Distributions for 800 KeV Electrons at L=5.4	23
12.	Pitch-angle Distributions for 400 KeV Electrons at L=6.5	24
13.	Pitch-angle Distributions for 800 KeV Electrons at L=6.5	25
14.	Electron Energy Spectrum before Flux Dropout	26
15.	Electron Energy Spectrum during Flux Dropout	27
16.	Electron Energy Spectrum after Flux Dropout	28
17.	Outer Magnetosphere Field before Compression, Projected to XZ Plane	29
18.	Outer Magnetosphere Field after Compression, Projected to XZ Plane	30
19.	Outer Magnetosphere Field after Compression, Projected to XY Plane	31
20.	Outer Magnetosphere Field after Compression, Projected to YZ Plane	32

(Continued on next page)

21.	Electron Motion before Compression, XY Projection and $\alpha_0 = 10^\circ$	33
22.	Electron Motion before Compression, XZ Projection and $\alpha_0 = 10^\circ$	34
23.	Electron Motion before Compression, YZ Projection and $\alpha_0 = 10^\circ$	35
24.	Electron Motion after Compression, XY Projection and $\alpha_0 = 10^\circ$	36
25.	Electron Motion after Compression, XZ Projection and $\alpha_0 = 10^\circ$	37
26.	Electron Motion after Compression, YZ Projection and $\alpha_0 = 10^\circ$	38
27.	Electron Motion before Compression, XY Projection and $\alpha_0 = 90^\circ$	39
28.	Electron Motion before Compression, XZ Projection and $\alpha_0 = 90^\circ$	40
29.	Electron Motion before Compression, YZ Projection and $\alpha_0 = 90^\circ$	41
30.	Electron Motion after Compression, XY Projection and $\alpha_0 = 90^\circ$	42
31.	Electron Motion after Compression, XZ Projection and $\alpha_0 = 90^\circ$	43
32.	Electron Motion after Compression, YZ Projection and $\alpha_0 = 90^\circ$	44
33.	Proton Motion before Compression, XY Projection and $\alpha_0 = 90^\circ$	45
34.	Proton Motion before Compression, XZ Projection and $\alpha_0 = 90^\circ$	46
35.	Proton Motion before Compression, YZ Projection and $\alpha_0 = 90^\circ$	47
36.	Proton Motion after Compression, XY Projection and $\alpha_0 = 90^\circ$	48
37.	Proton Motion after Compression, XZ Projection and $\alpha_0 = 90^\circ$	49
38.	Proton Motion after Compression, YZ Projection and $\alpha_0 = 90^\circ$	50
39.	Recovery Phase Pitch-angle Distributions for 400 KeV Electrons	51
40.	Recovery Phase Pitch-angle Distributions for 800 KeV Electrons	52

Accession For
 NTIS GRA&I ☒
 DTIC TAB ☐
 Unannounced ☐
 Justification _____

By _____

Distribution/ _____

Availability Codes

Dist	Avail and/or Special
A-1	

1. Introduction

This report summarizes the scientific and technical progress made during the 12-month duration May 1, 1990 through May 31, 1991 under the subject contract.

Since this is the initial year of the contract and CRRES science data usable for modeling were not available until about September 1990, our modeling effort up to the present is limited to infrastructure and single cases of dynamic storm effects, as specified in the original proposal. The major efforts on a storm time model with statistical support await the formation of an outer belt storm data base, which is being accumulated currently. In spite of the short time interval since initiation, at least four significantly new results in basic magnetospheric science have been obtained under the auspices of this contract. These are: (1) a complete and exact solution of the outer magnetosphere with properties that mimic the bow shock, the magnetosheath, the magnetopause and IMF merging for any given shape of the magnetopause and bow shock boundaries; (2) discovery of the general properties of high-energy (~ 1 MeV) electron and proton encounters with the outer magnetospheric structures, leading to a computer verification of the concept of outer radiation belt particle recycling by geomagnetic storms; (3) new interpretations for the causes of the violent fluctuations of outer belt electron fluxes as results of insights gained in (1) and (2) above; and (4) a new integral view of the initial and recovery phases of outer belt dynamic responses to geomagnetic storms. The last item is the result of insight from our current examination of CRRES data in the context of our theoretical development. Although it is too early to determine if the modeling strategies developed hitherto may or may not require major modification, as result of compiling a sufficient stormtime data base; it is significant to note that, up until this effort organized by the CRRES program, there has not been an attempt to develop an integrated model of the dynamical response of the outer electron belt in the context of magnetic storms, in a quantitative manner according to the response times of its phases.

In this report, we shall attempt to give a scientific overview of the current modeling strategy, rationale and observational motivation, as if the theoretical approaches are well established. This by no means implies that we shall not modify the modelling approaches in response to the accumulating CRRES data base. Rather, we believe that, unless we commit ourselves to the test of a specific organized conceptual modelling scheme, the well-established violent fluctuations of the outer belt will not be easily unravelled.

The main body of this report is divided into 6 sections: (2) Outer Magnetosphere

Modeling, for establishing an infrastructural context for viewing the outer belts; (3) Diffusion Modeling, for studying responses on the time scale of days; (4) Particle Encounters with Outer Magnetosphere Structures, for studying responses on the drift time scale; (5) Test Case; (6) Future Work; and (7) Publication and Presentation List.

2. Outer Magnetosphere Modeling

To determine the response of the outer belt, it is necessary to have a model of the outer magnetosphere that mimics the magnetospheric response to solar wind parameters. An outer magnetosphere model must include the responses of the outer magnetosphere structures such as bow shock, magnetopause, magnetosheath and merging efficiency parameterizations. There is currently no such basic physics model as the detailed plasma physics are still being determined. There are magnetohydrodynamic and potential field solutions which represent the current state-of-the-art; all of these models require CRAY-like computation requirements with long running times. Such models are scientifically significant but entirely impractical in the context of usage for outer belt dynamic modeling based on CRRES data; since the role of the outer magnetosphere model is to serve as part of the infrastructure for the dynamical motion of energetic particles. On the other hand, the reality is that, without a reasonable analog of the outer magnetosphere structure, especially on the dayside, little organized progress can be made in the context of CRRES data interpretation.

Stern (JGR, 1986) described an elegant approach to the magnetosphere modeling problem by demonstrating that the difficult potential boundary value problem can be simplified by choosing a co-ordinate system in which the magnetospheric boundary structures, such as bow shocks or magnetopauses, lie on a co-ordinate surface. He demonstrated how an elegant inner magnetosphere solution with appropriate currents to yield a paraboloidal magnetopause can be specified efficiently with an expansion of the paraboloidal eigenfunctions for Laplace's potential equation.

In the first phase of our outer magnetosphere modeling effort, we adopted this approach to obtain exact solutions that include paraboloidal outer magnetospheric structures (bow shock and magnetopause), including dayside merging of the IMF and the internal geomagnetic field represented by an efficiency parameter. The price paid for such an elegant solution is that the shapes of outer magnetospheric structures are restricted to be on a co-ordinate surface; and, in addition, tail effects are ignored. The latter drawback is not serious for outer belt modeling because the outer belt does not extend to L -values

much higher than 8. Figure 1 summarizes the mathematics involved. Figure 2 shows a typical sample of the exact potential solution result that is virtually indistinguishable from magnetohydrodynamic calculations requiring extensive computational resources. We have used this paraboloidal outer magnetosphere code to mimic dayside outer magnetospheric structures for various test-case scenarios which we will discuss in Section 4 and 5.

The paraboloidal outer magnetosphere model has the virtues of simplicity and timeliness for study of the first results of CRRES outer radiation belt data. Its elegance as an exact solution has intrinsic scientific value; however, two major elements need to be accommodated: (1) a magnetosphere inside the magnetopause with a tail structure and (2) a non-paraboloidal magnetopause shape which is consistent with observations and with the existence of a tail. While there are several such magnetosphere models available to be accommodated into our development of the outer magnetosphere boundary conditions, the development of the Source Surface Model (SSM) prescription by Schulz and McNab (GRL 1989) has the virtue that it can accommodate arbitrary magnetopause shapes and their appropriate tail currents. We have recently initiated a merger of the Outer Magnetosphere Potential Model with the Source Surface Model. The results of this merger are very satisfactory.

Figures 3 and 4 show such implementations for a paraboloidal bow shock and a magnetopause shape that fit observations well. Only outer magnetosphere field lines are shown in these cases for simplicity. Computation requirements for this type of model are about one order of magnitude higher than the paraboloidal model; however, it is still economical compared to magnetohydrodynamic solutions. This work is in collaboration with Mike Schulz, who is not supported by the subject contract. An invited paper on this significantly new development in basic magnetosphere physics will be presented by Mike Schulz in the IAGA meeting in Vienna in August 1991. A detailed paper, under the leadership of Lockheed and the sponsorship of this subject contract, is being prepared for publication. Because of the heavy computation requirements, development of this model is partially funded by the Lockheed Independent Research Program in addition to the subject contract.

3. Diffusion Modeling

A reasonable outer magnetosphere model that mimics its response to solar wind conditions is an essential infrastructure element in dynamic modeling of the outer belt. The other essential element is an efficient accounting of the particle diffusion processes that are expected to take place in the re-establishment of the equilibrium after the initial storm

response.

In the fore-runner study with SCATHA/SEP data, we demonstrated that simultaneous radial and pitch angle diffusions can account for the behavior of outer electron belt dynamics on the time scale of a day or so. The physical diffusion parameters derived from the SCATHA high energy electron data are in good agreement with other independent determinations and theoretical expectations. For CRRES dynamic modeling, we make use of this facility that has been constructed in the last three years. The principles of the diffusion modeling have been published in two detail papers [JGR 93, 2619, 1988; JGR 95, 12069, 1990].

Although the basic assumptions and applications of the simultaneous radial and pitch angle diffusion model are the same between the SCATHA tests and the CRRES applications, there is still a major difference that needs to be addressed. The cases treated in the SCATHA data base are in moderate geomagnetic activity without consideration of drift-time scale responses to clearly defined geomagnetic storms; whereas, the main objective of the CRRES storm response model is to attack the outer belt response to storms at all time scales.

Aside from issues such as the geomagnetic field, the diffusion response in the recovery phase of the response model requires an additional term on the right hand side of the diffusion equation; namely,

$$\frac{\partial f}{\partial t} = \Delta f + \frac{F(L, x, t)}{\tau} \quad (1)$$

where Δ is the simultaneous radial and pitch angle diffusion operator specifying the time rate of phase space density change ($\frac{\partial f}{\partial t}$) due to diffusive processes. The new term, with time scaling τ , represents a "source" term due to non-diffusive time rate of change of phase space density (F). In this regard, the nomenclature "source" is a misnomer originating from tradition, which sweeps anything unaccounted for by diffusion as a "source". In our storm time response model, for example, parts of this source term can be the population of outer belt electrons removed to the outer magnetosphere by non-diffusive processes such as scatterings on drastically changed magnetospheric structures. The recycling of such populations into the usual outer belt location by radial diffusion during the recovery response of the outer belt is represented in the diffusion equation as a particle source of non-diffusion origin. The objectives of a dynamic modeling effort, aside from deriving diffusion parameters (properties of Δ), is to specify the "source" term that would account

for the properties of a CRRES storm data base, which is currently being accumulated. At the present time, several interesting aspects of F have been revealed by examining the detailed phase space density of a test case (storm of August 1990), which is discussed in Section 5 in more detail.

Meanwhile, the computational procedure to unravel the diffusion equation (1) to specify the diffusion parameters of Δ and to construct the appropriate F requires decomposition of the observed distribution function f into eigenfunctions of Δ so as to facilitate extraction of the diffusion constants. Since we have chosen an approximate representation of Δ such that its eigenfunctions are also a complete set in pitch-angle space, the rendering of CRRES data in terms of (1) requires the first step of decomposing f into pitch-angle eigenfunctions that allows us to reduce the independent dimensions of (1) by one. The critical test of this step is whether the pitch angle decomposition of f into approximate pitch-angle eigenfunctions (Bessel functions of order zero) is as efficient as the SCATHA test cases. It is noted that the CRRES modeling case requires this decomposition throughout the storm phases. We demonstrated this decomposition in Figures 5 and 6.

In Figure 5, the pitch-angle decomposition amplitudes Q_n in

$$f = \sum_n Q_n \left[\delta_{n0} + (1 - \delta_{n0}) \frac{\sqrt{2} J_0(k_n x/x_c)}{x_c J_1(k_n)} \right] \quad (2)$$

is shown for the entire CRRES orbits of 77 (initial storm response) and 82 (late recovery response) for electron energy channels 800 keV and 400 keV respectively. The dependence of these amplitudes Q_n upon L need not concern us for the moment. The important point is that in the outer belt the amplitudes of the $n = 0 - 4$ modes account for the total of (2), even for the violently changing initial response (orbit 77).

We have completed the pitch angle decomposition of the data base (orbits 76-82) for the sample storm of August 1990 and found the decomposition to be rapidly and stably decreasing with order. As in the SCATHA tests, 4 orders of pitch angle eigenfunctions are quite sufficient to decompose the CRRES test case above.

4. Particle Encounters with Outer Magnetosphere Structures

A third infrastructural element is required to examine the behavior of the outer belt in the initial response to geomagnetic storm conditions. The fact that the dayside magnetosphere is highly distorted in the storm initial phase is evident and discussed in Section

2. Of chief interest to outer belt dynamic modeling, however, is how do the trapped energetic particles move in the distorted outer magnetosphere on the drift and bounce time scales? The answer to this question is crucial to the description of the initial phase of a dynamic response model and to construction of the non-diffusive "source" function F for the recovery phase.

Crucial as the description of energetic particle encounters with the outer magnetospheric structures may be, it is also unfortunate that there is no economical method to study the properties of f , as an ensemble, except to examine and generalize the behavior of individual particle traces in terms of a simulation. We have done extensive studies in this area at the early part of this contract year while awaiting CRRES data to accumulate.

We have accumulated an extensive computation data base of MeV electron and proton trajectories of various initial pitch angles moving in paraboloidal outer magnetospheres such as those shown in the next section. In addition, we have also included outer magnetospheres with superimposed large scale wave structures in the computational trajectory data base. This large data base of trajectories cannot be conveniently exhibited here because of variations in initial pitch angle and outer magnetosphere geometry; therefore, the samples shown in the next section for specific outer magnetospheres are more appropriate samples to indicate the inventory of our study results in this area. Here, we state several general conclusions that are applicable to MeV particle motion even outside of the context of outer belt modeling:

(1) MeV particle encounters with outer magnetosphere structure, as simulated by our paraboloidal magnetopause, magnetosheath and bow shock, rarely lead to loss of the particle into the dayside heliosphere.

(2) The most common result of such encounters leads to scatter of the particle trajectory from tightly defined trapped bounce-drift motion to quasi-bounce-drift motion steered by the outer magnetosphere structure on trajectories that span a much larger volume of space but mostly inside the magnetosphere. The immediate consequence of this feature is the dispersal of outer belt fluxes to a low level in those populations of the outer belt that have encountered the outer magnetosphere.

(3) Electrons (protons) invariably enter the magnetosphere on the dawn side (dusk side) and leave on the dusk side (dawn side).

(4) Since outer magnetosphere models used in this series of studies do not contain a tail, the effects of the geomagnetic tail structure to MeV particles is not revealed here.

Other studies at lower energy also indicate scattering but, again, contained inside the magnetosphere.

The reader is referred to Section 5 for detailed ramification of these conclusions in terms of the specific test case of the August 1990 storm.

5. Test Case: Storm of August 1990

Despite the small magnitude of geomagnetic activity associated with the storm of August 1990, its effects on the outer magnetosphere and the advantageous location of CRRES on the mornside side flanks of the magnetosphere combined to yield distinctive features that, in our opinion, have sharpened our understanding of the outer belt dynamic response to solar wind conditions. This section, as well as the major part of our interpretation and modeling effort in the latter half of the contract period, is devoted to this storm, not only as a sample of our standard modeling procedure that will be applied to every storm of our accumulating CRRES Storm Data Base, but also as a stand-alone science analysis project since we are able to isolate several new features of the outer belt response. The first part of this section deals with the organized SEP data base for this event while the second part deals with modeling the initial phase of the outer belt dynamic response. The recovery phase of the response has yet to be modeled.

a. SEP Data for the Event

The solar wind conditions for the event is capsulized in Figure 7 which shows the subsolar standoff distances of the magnetopause and the IMF components as the initial phase of the event progresses. The standoff distance shows two sudden inward motions. We have used the information in this figure to define analogous outer magnetosphere models for both inward motions of the standoff and distance. Only results of the second inward motion (to $L = 6.5$) will be discussed here since immediate responses of the outer belt energetic electrons are observed by CRRES in its apogee region shown on Figure 8. The electron flux spectographs, Figure 9, show the electron fluxes of the SEP instruments for orbits 75 (before the event), 77 and 79, ordered by L-value. Focusing upon the energetic band (above 200 keV), it is quite clear that a "drop-out" of flux was detected within the drift time scale (less or order of one hour). Recovery to pre-event fluxes for these particles had not occurred one day later. Indeed, it took 2-3 days before complete flux recovery. The short time scale of the flux drop out is the first notable feature because it clearly does not indicate a diffusion process.

Next, the pitch angle characteristics of the energetic electrons also yield significant insight into the dynamics of the dropout. Figures 10-13 is a set of pitch angle distributions measured on orbit 77 at two L-values before (inbound) and after (outbound) the flux drop out mapped to the equator for uniformity of comparison, as indicated by the flux levels for both the 400 keV and 800 keV channels. Two important features are apparent when the set is examined as a whole. First, the inbound (before) pitch-angle distribution exhibits the usual pitch-angle diffusion signature sloping towards smaller pitch angles; whereas all the outbound (after) distributions are isotropic up to the loss cone. The dynamical process responsible for the flux drop out must be able to isotropize the pitch-angle distribution within a time less than 3 hours shown on the $L = 6.5$ pair, Figures 12 and 13. That the flux drop out process is temporal is also clearly indicated by the examining the magnetic local time (MLT) differences of the inbound and outbound fluxes. The "before" and "after" states are clearly marked within a distance of 1.5 hour MLT. A diffusive or convective process that can produce a flux decrease of 800 keV electrons of up to an order of magnitude within a spatial extend of 1.5 hour MLT is difficult to imagine. We suggest a scattering process such as described in the previous section and analogously modeled in the latter part of this section.

Another important characteristic of the outer belt electrons above 400 keV before, during and after the flux drop out is revealed in the set of Figures 14, 15 and 16. These spectra in the energy interval 400 keV to about 1.5 MeV exhibit the same decrease of roughly 1.5 decade of flux. Apparently, the dynamics of the flux drop out does not effect the spectrum in this energy range which is the concern of our model. The level of multi-MeV electrons also seem to remain constant, i.e. does not participate in the drop out, and the spectra of the low energy electrons are drastically different in these Figures. The latter can be due to dB/dt (inductive electric field effects), but the unchanged spectra of the high energy electrons do not fit the inductive electric acceleration hypothesis as the amount of acceleration is proportional to the initial energy of the particle, thus resulting in spectrum changes.

The only hypothesis that agrees with all of the above observed features that we have been able to come up with is that of scattering of the outer belt population giving rise to an increased volume in which the population is contained. The scatterings with outer magnetosphere features can reasonably isotropize the pitch angle distribution in a short time without affecting the spectrum.

b. Analogy Modeling for the Event

In this segment, the entire effort was focused on analogy modeling for the initial part of the outer electron belt and trapped proton response to the storm of CRRES orbit 77. During this period, the outer magnetosphere is very dynamic. The dynamic response time scale of particle distributions is considerably shorter than normal diffusion times; therefore, a diffusive picture is not appropriate for these initial orbits. This view is clearly supported by observations cited in the previous segment.

The focus of the modeling effort is to present a clear picture, for the first time as we can determine to date, of the initial response of the outer radiation belt to sudden changes of solar wind flow and magnetic parameters. We are using the storm as a benchmark for our outer-belt dynamic modeling work. At the present time, sufficient details of our data analysis and parallel simulation work have emerged to afford a strikingly exciting and new view of radiation belt processes occurring in the outer magnetosphere. We shall present a series of charts here to document the current state of several parallel segments of the initial storm response modeling effort. The segments of data and modeling are shown in a logical sequence, as follows:

1. Solar wind stand-off distance and IMF data
2. Outer magnetosphere model with paraboloid magnetopause and bow-shock corresponding to the solar wind data.
3. The storm response data indicating an extensive "drop out" of outer belt flux.
4. Study of radiation belt electron and proton motion in the region affected by the sudden movement of the magnetopause inward.

Taking averages of the standoff distance and IMF components for a period of about 3 hours before and after the second sudden change of Figure 7, we arrived at critical parameters to model the outer regions of the magnetosphere. Figure 17 shows the X-Z plane projection of our open outer magnetosphere model with merging efficiency of 0.2 from the period before the sudden compression. The IMF component values are shown at the top. The outer magnetosphere model is an exact solution of Laplace's equation with a paraboloidal shape that fits the observed average stand off distance and IMF magnitude parameters.

Figures 18, 19 and 20 give the three orthogonal projections of the outer magnetospheric field after the sudden compression. The IMF components and other parameters are given at the top. Comparisons of Figures 17 and 18, 19 and 20 show the drastic changes of the outer magnetosphere configurations.

To model what happens to radiation belt particles trapped in the region of dynamic change, the vicinity of 6-8 RE as measured on the dayside, we investigate the dynamical behavior of such particles (10 MeV electrons and protons for the sake of reducing computer running time) before, during and after the outer magnetosphere configuration change.

We have made many runs of electron and proton trajectories. The following is just a sample that brackets 0 and 90 degree equatorial pitch angles. The trajectories were started at 90 degree pitch angle near the mirror point of field lines that were just inside of the magnetopause to assure "classical" trapping or "scattered" trapping ("rattling along the magnetopause inside") that we have discussed in previous reports. Depending on minor differences of the starting pitch angle, the particles "fen out" into equatorial pitch angles of 0-90 degrees. The parameters of each set of three projections per sample trajectory are printed at the top of each figure.

Figures 21, 22 and 23 show the projections of an electron trapped in the "Before" outer magnetosphere with equatorial pitch angle of about 10 degrees. This particle is very near the "Before" loss cone. Figures 24, 25, 26 show the same projections of the same particle in the "After" outer magnetosphere. It is seen that it did not bounce even once before it went off into the tail region. Since our outer magnetosphere model is not expected to be good in the tail, we cannot comment on the fate of this particle.

Figures 27, 28, 29 depict projections of an electron with equatorial pitch angle near 90 degrees in the vicinity of 6RE near the morning dayside in the "Before" magnetosphere. Figures 30, 31, 32 depicts the same particle in the "After" magnetosphere. It is seen that this particle, in the vicinity of CRRES, is scattered into the quasi-trapped trajectory "rattling" near the inside wall of the magnetopause. Considering that this particle has 90 degree equatorial pitch angle before, the "drop out" of flux in the $L=6$ region shown in Figure 9 is easily understood. The important point, however, is that this particle is not lost to the magnetosphere. It is merely dispersed into the "rattling" trajectory. Later, perhaps much later as our flux drop out did not get filled in completely even after Orbit 84, this particle can be recycled back into the outer belt by diffusive processes.

The next set of figures investigate the effects of the sudden decrease of the magnetopause standoff distance upon a stably drifting particle. Because of the long computation time for electrons, we use a 10 MeV proton as test particle. Figures 33, 34, and 35 shows the stably drifting trajectory of the proton in the "Before" outer magnetosphere. Note that this particle has equatorial pitch angle in the 45 degree region. After the decrease of

the standoff distance, shown in Figures 36, 37, and 38 we see that the stable drift persists except that it now "rattles" along the magnetopause on the dayside, staying on some of the time in the magnetosheath.

Conclusion: We have made a great deal of progress understanding the initial response of the outer belt to magnetic storms by modeling both the magnetic field and particle behavior of the selected CRRES event. Solar wind data is absolutely necessary to achieve this. This flux "drop out" at the initial phase of the magnetic storms is likely to be understood as a dispersal of the trapped outer belt by scattering with outer magnetospheric structures. Diffusive processes operate over much longer time scales later to fill in the void left by scattering.

c. Recovery Phase

As indicated previously, the diffusion model for the recovery phase of the event is currently underway. Figures 39 and 40 show the pitch-angle distributions typical of diffusion. Further, these figures with fluxes from inbound, outbound and the two halves of the magnetic field lines mapped to the equator show unequivocally that there are no local-time or temporally sudden processes in operation.

6. Future Work

In the above, we have outlined the salient observational features of the CRRES/SEP outer belt dynamic data especially in the context of storm responses. Further, we have put together a plausible modeling hypothesis to organize the significant features of these data into the proto-type of an outer belt dynamic model. As for the validity of this model, its tests against data will be the final arbiter.

Meanwhile, our preliminary work summarized here needs to be completed in the following principal areas:

- a. Completion of diffusion work throughout the data of the event.
- b. Examine the effects of outer magnetosphere scattering upon fluxes and spectra.
- c. Incorporate usage of more realistic geomagnetic fields that include tail and better-modeled magnetopauses.
- d. Compile a storm data base, using the August 1990 storm as benchmark.
- e. Determine short-term storm response of the outer belts from by phenomenological and theoretical points of view.
- f. Initiate final phase of outer belt dynamic modeling as specified in the proposal.

7. Publications

1. Y. T. Chiu, M. A. Rinaldi, and R. W. Nightingale, Toward dynamic modeling of the outer electron radiation belt, *J. Geophys. Res.*, 95, 12069, 1990.
2. Y. T. Chiu, W. E. Francis, and M. Schulz, An exact potential model of the outer magnetosphere, *J. Geophys. Res.*, in preparation, 1991.
3. Y. T. Chiu, M. A. Rinaldi, W. E. Francis, R. M. Robinson, and R. W. Nightingale, Outer magnetosphere and radiation belt particle dynamics in the storm of August 26, 1990, Invited paper, American Geophysical Union Spring Meeting, June 1, 1991.
4. M. Schulz, Y. T. Chiu, and W. E. Francis, A model of the outer magnetosphere, Invited paper, IUGG General Assembly, August 12, Vienna, Austria.

MAGNETOSPHERE IN PARABOLOIDAL HARMONICS

LAPLACE EQUATION : $\nabla^2 \Phi = 0$

$\vec{B} = -\nabla \Phi$

GENERAL SOLUTION :

$$\Phi = \sum_n \sum_m \frac{\sin m\phi}{\cos m\phi} J_m(k_n \mu) [a_m(k_n) I_m(k_n \lambda) + b_m(k_n) K_m(k_n \lambda)]$$

INTERIOR REGION (TO MAGNETOPAUSE $\lambda = \lambda_p$)

$$a_m \neq 0 ; b_m = 0$$

MAGNETOSHEATH :

$$a_m \neq 0 ; b_m \neq 0$$

EXTERIOR REGION (TO BOW SHOCK $\lambda = \lambda_s$)

$$a_m = 0 ; b_m \neq 0$$

Figure 1

BOW SHOCK & OPEN MAGNETOPAUSE FIELD LINE TRACE
 DATE= 8-APR-91, SOLAR WIND ($V = 1403$ Km/s, $N = 5$ 1/cm³)
 EXTERIOR (B_x, B_y, B_z) IS $(-10.0, 0.0, 0.0)$ nT, $E = 0.20$
 MAGNETOPAUSE VALUES N_T, X_M, Z_M & A ARE: 20, 6.3, 10.0, 10.
 FIELD LINE IN (X,Z) PLANE, DIPOLE TILT= 0.0 DEG.

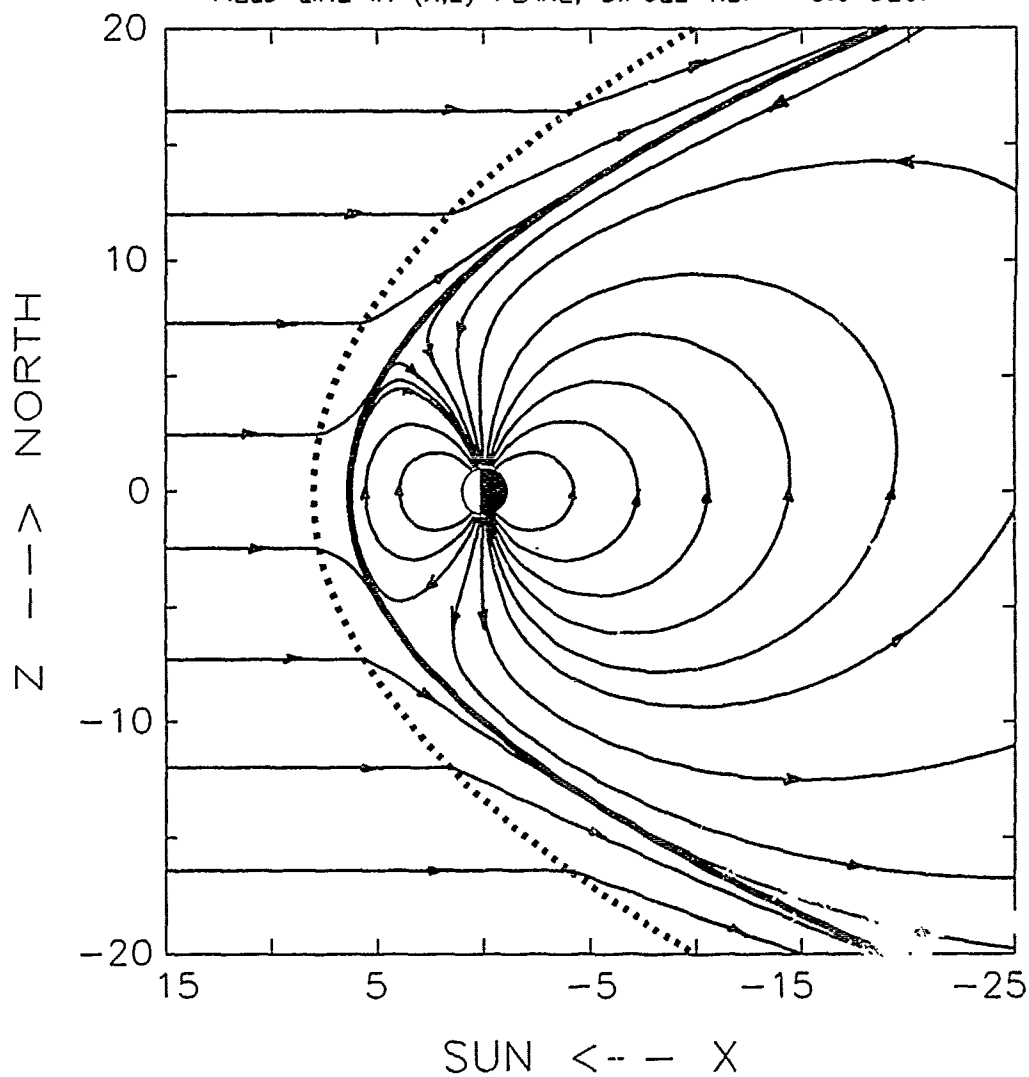


Figure 2

FIELD LINE TRACES OF NEW "SSM" MAGNETOPAUSE
 DATE= 5-JUN-91, SOLAR WIND ($V = 254 \text{ Km/s}$, $N = 10 \text{ 1/cm}^3$)
 EXTERIOR (B_x, B_y, B_z) IS $(-10.0, 0.0, 0.0)$ $E = 0.00$
 MAGNETOPAUSE VALUES NT, X_S, X_M & X_{LIM} ARE: $12.6, 10.0, -30$
 FIELD LINE IN (X,Z) PLANE, DIP: 12.6 DEG.

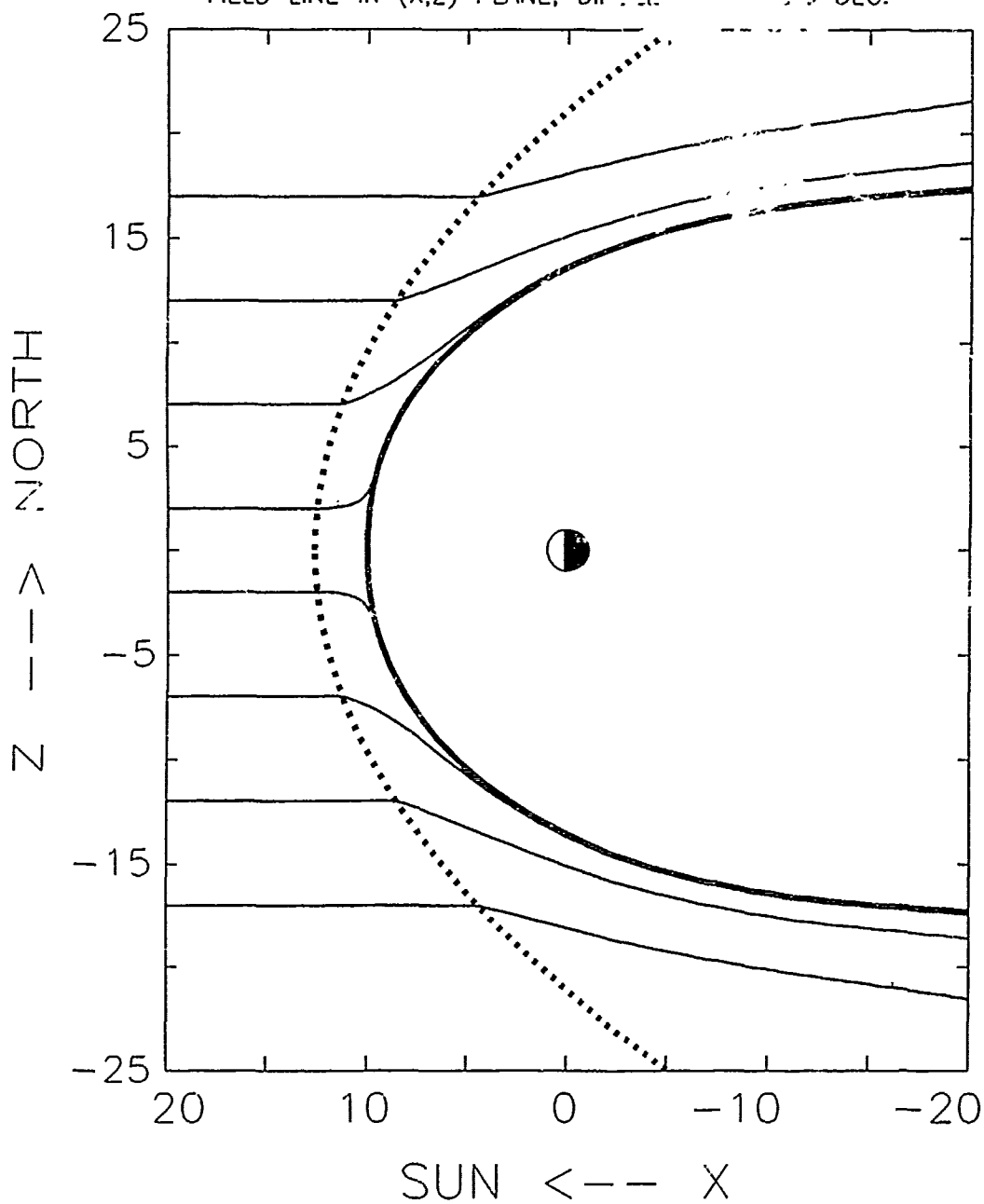


Figure 3

CLOSED "SSM" FIELD LINE TRACES NEAR MAGNETOPAUSE
 DATE=14-JUN-91, SOLAR WIND ($V = 254 \text{ Km/s}$, $N = 10 \text{ 1/cm}^3$)
 EXTERIOR (B_x, B_y, B_z) IS (0.0, 0.0, 10.0) nT, $E = 0.00$
 MAGNETOPAUSE VALUES NT, X_S, X_M & X_{LIM} ARE: 15, 12.6, 10.0, -70
 FIELD LINE IN (X,Z) PLANE, DIPOLE TILT= 0.0 DEG.

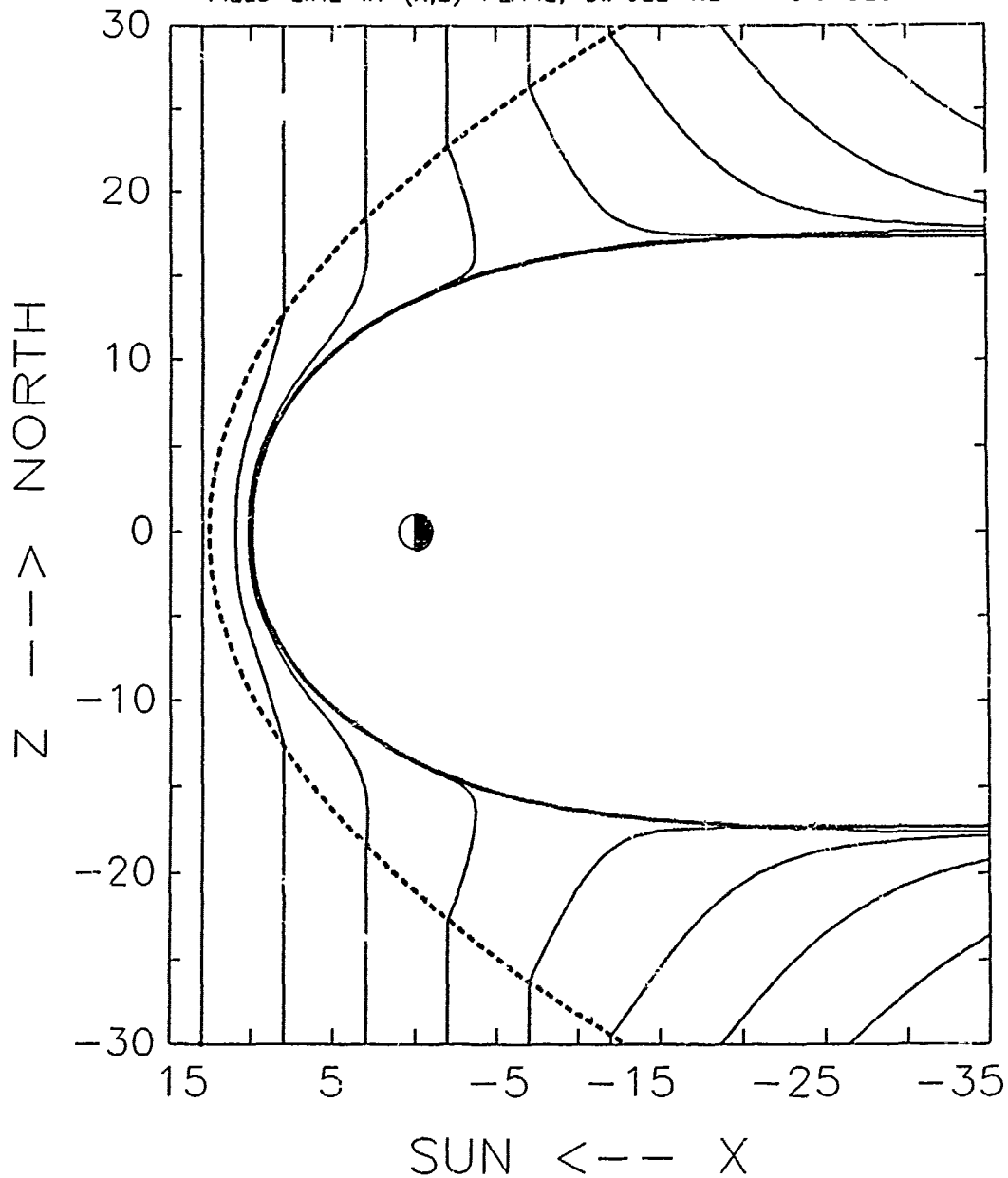


Figure 4

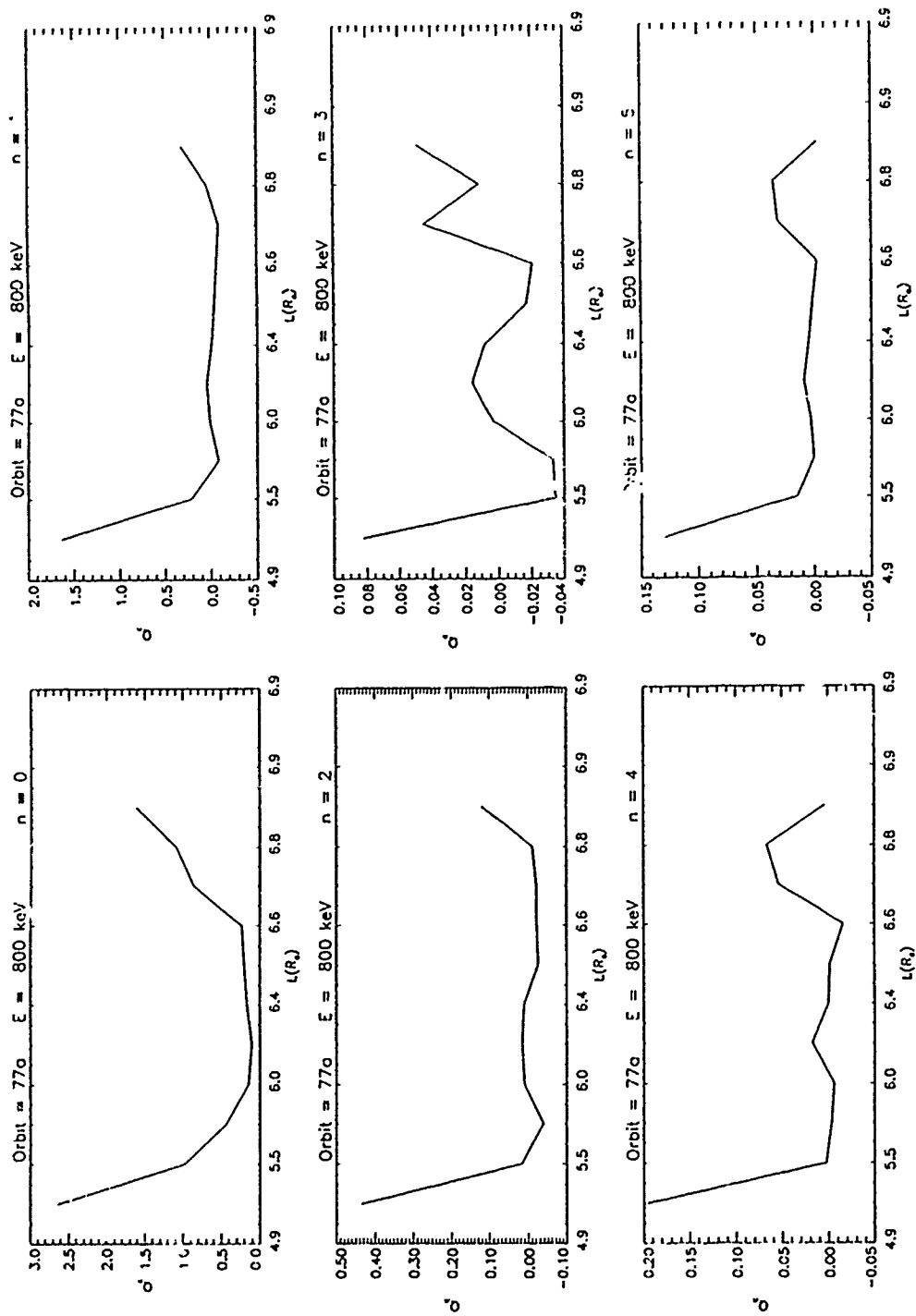


Figure 5

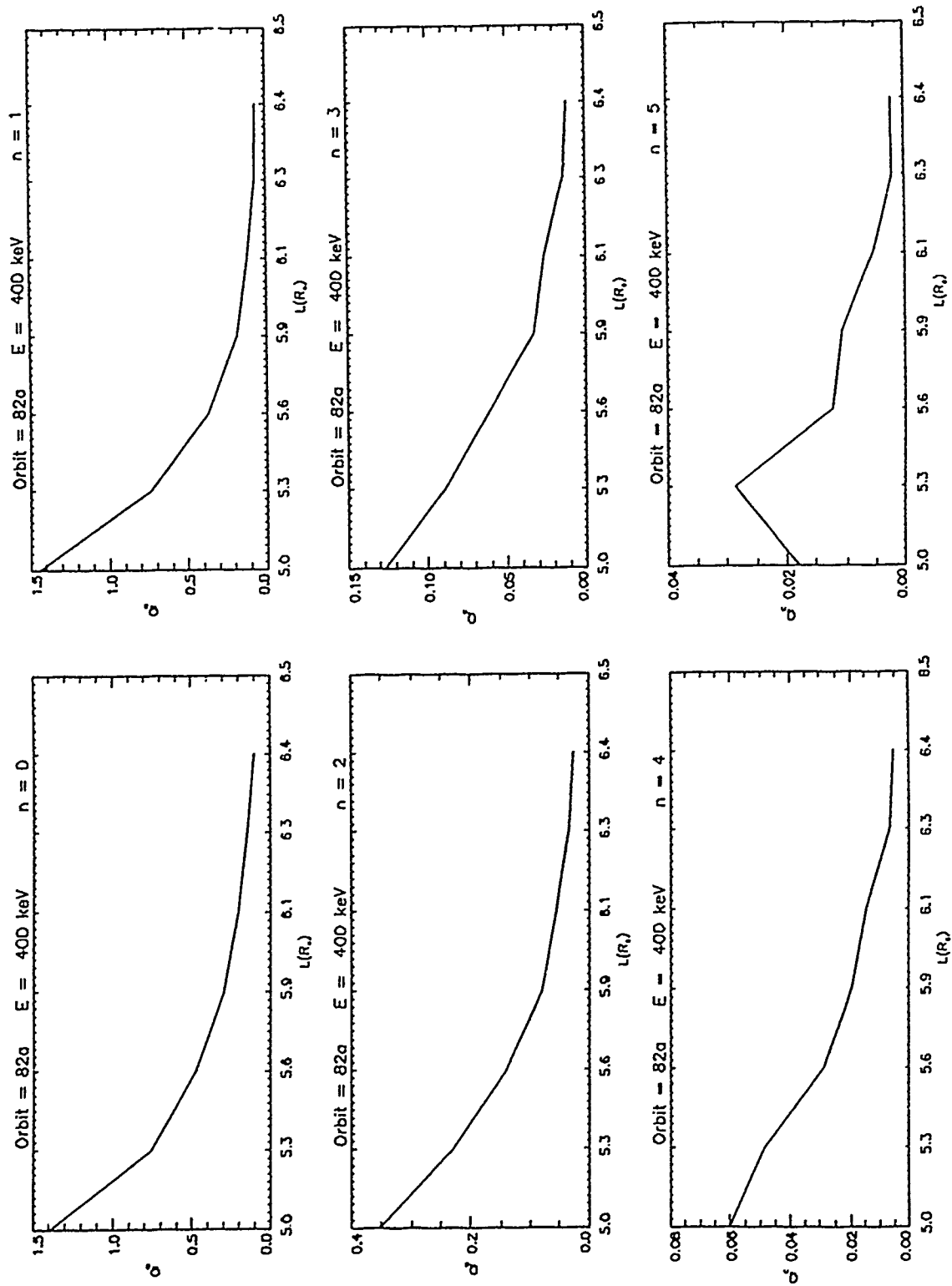


Figure 6

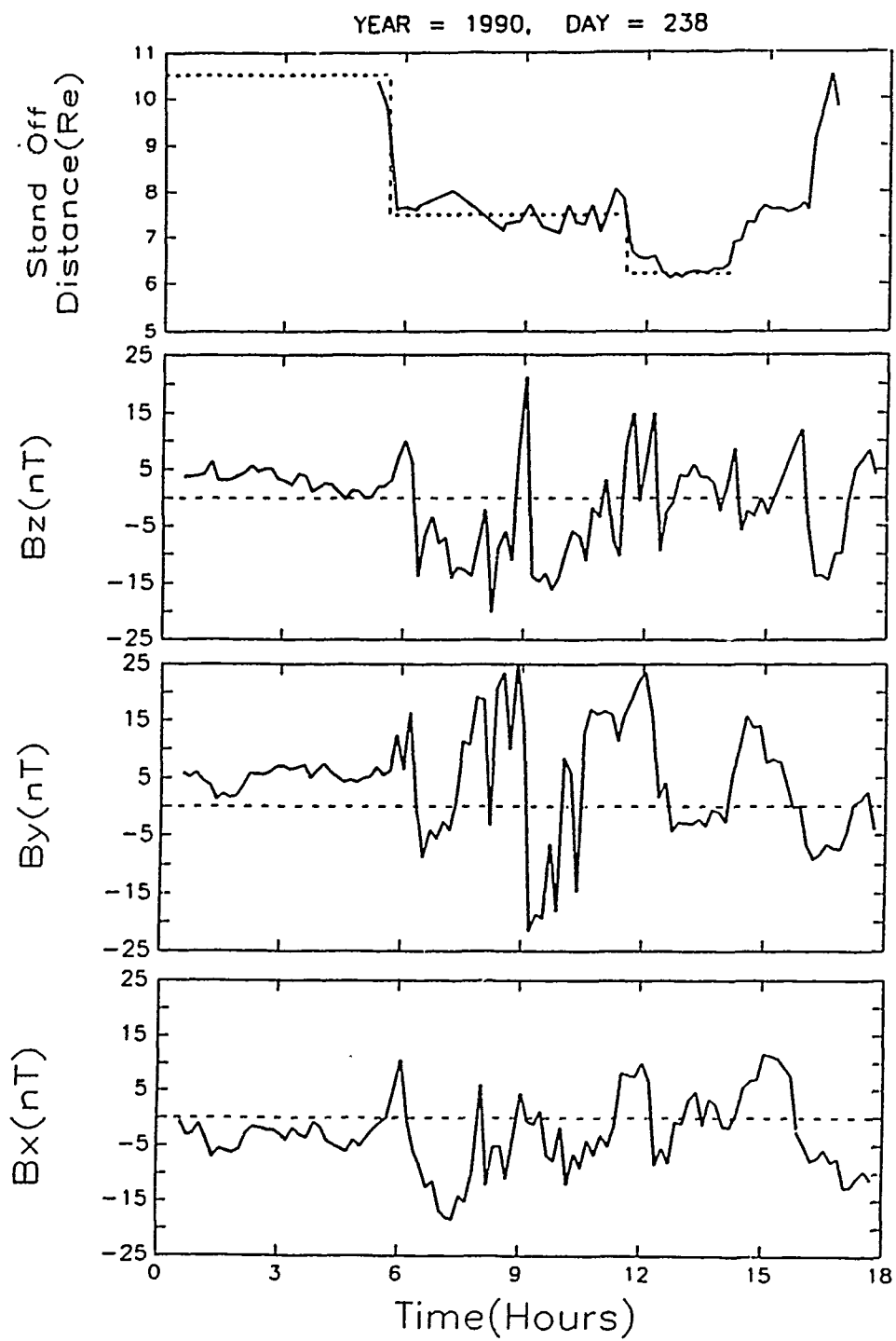


Figure 7

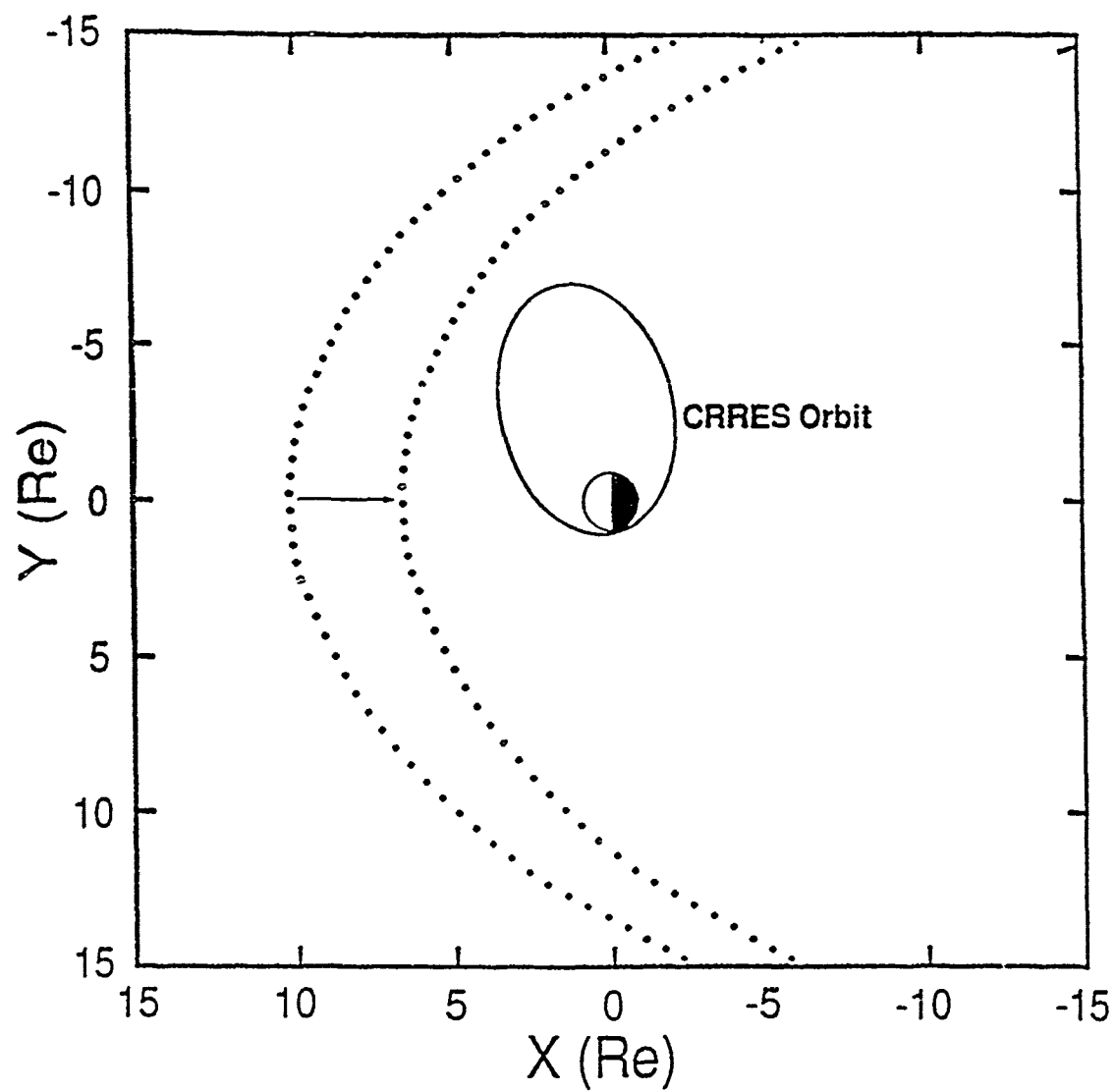


Figure 8

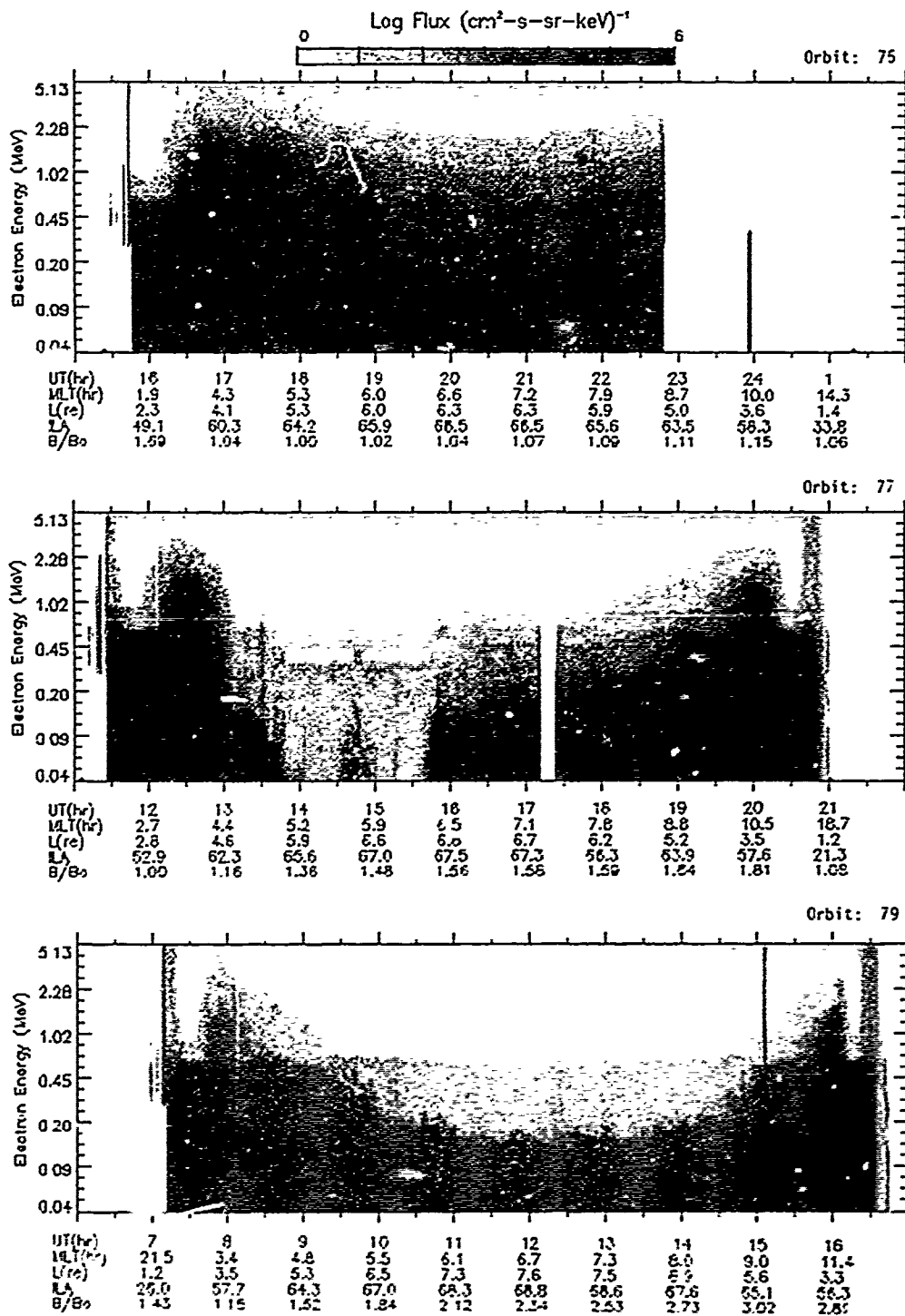


Figure 9

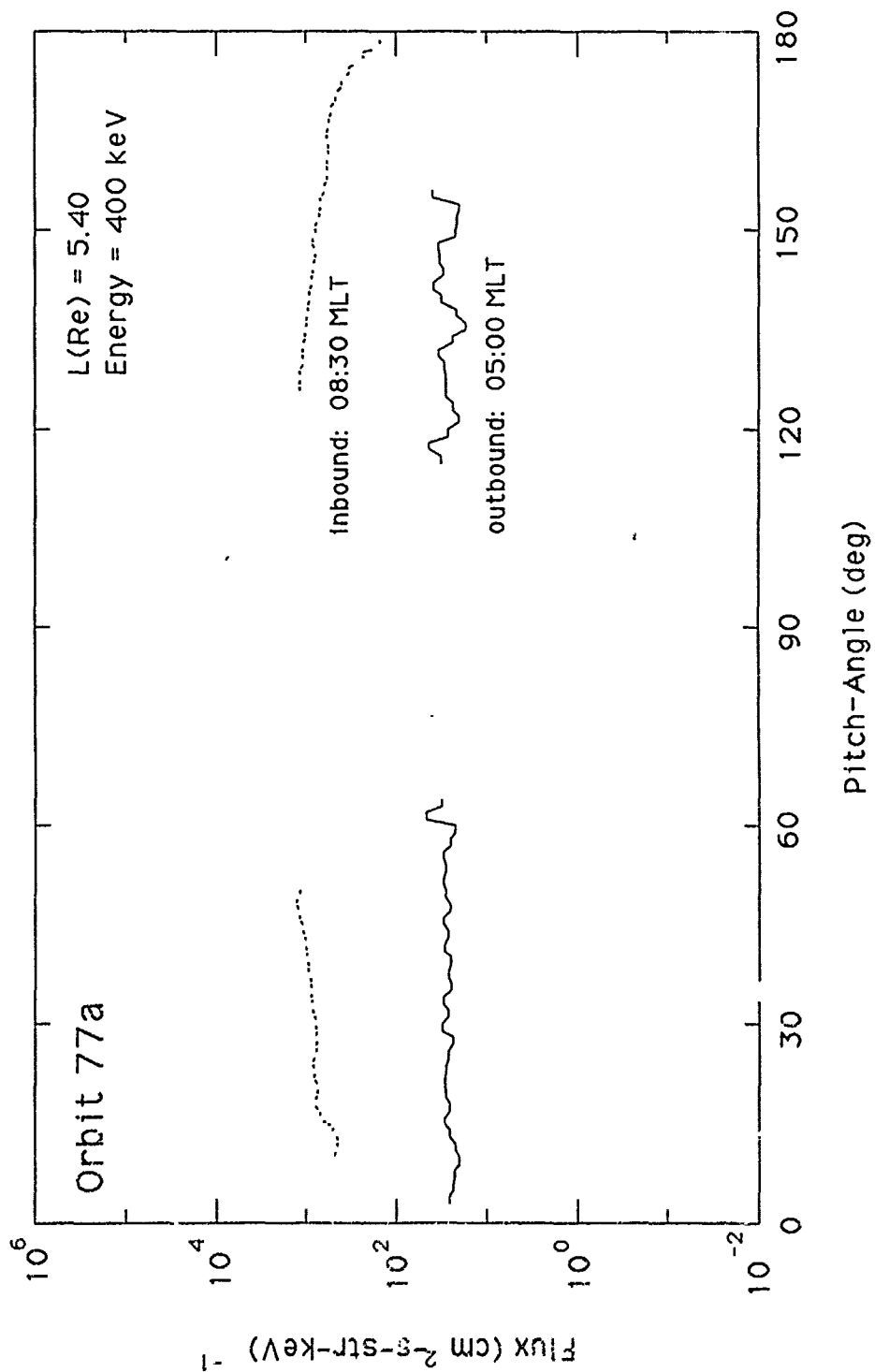


Figure 10

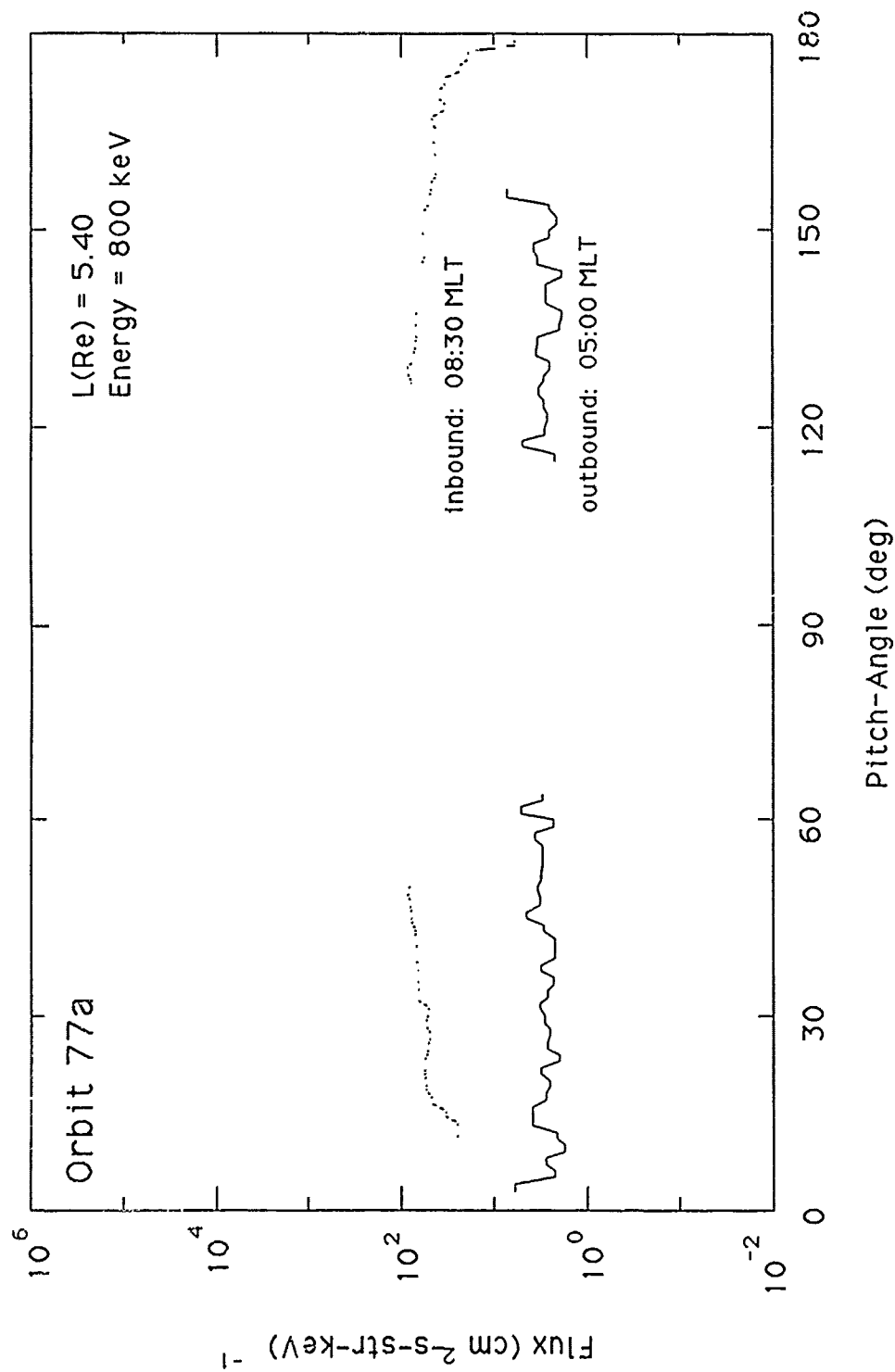


Figure 11

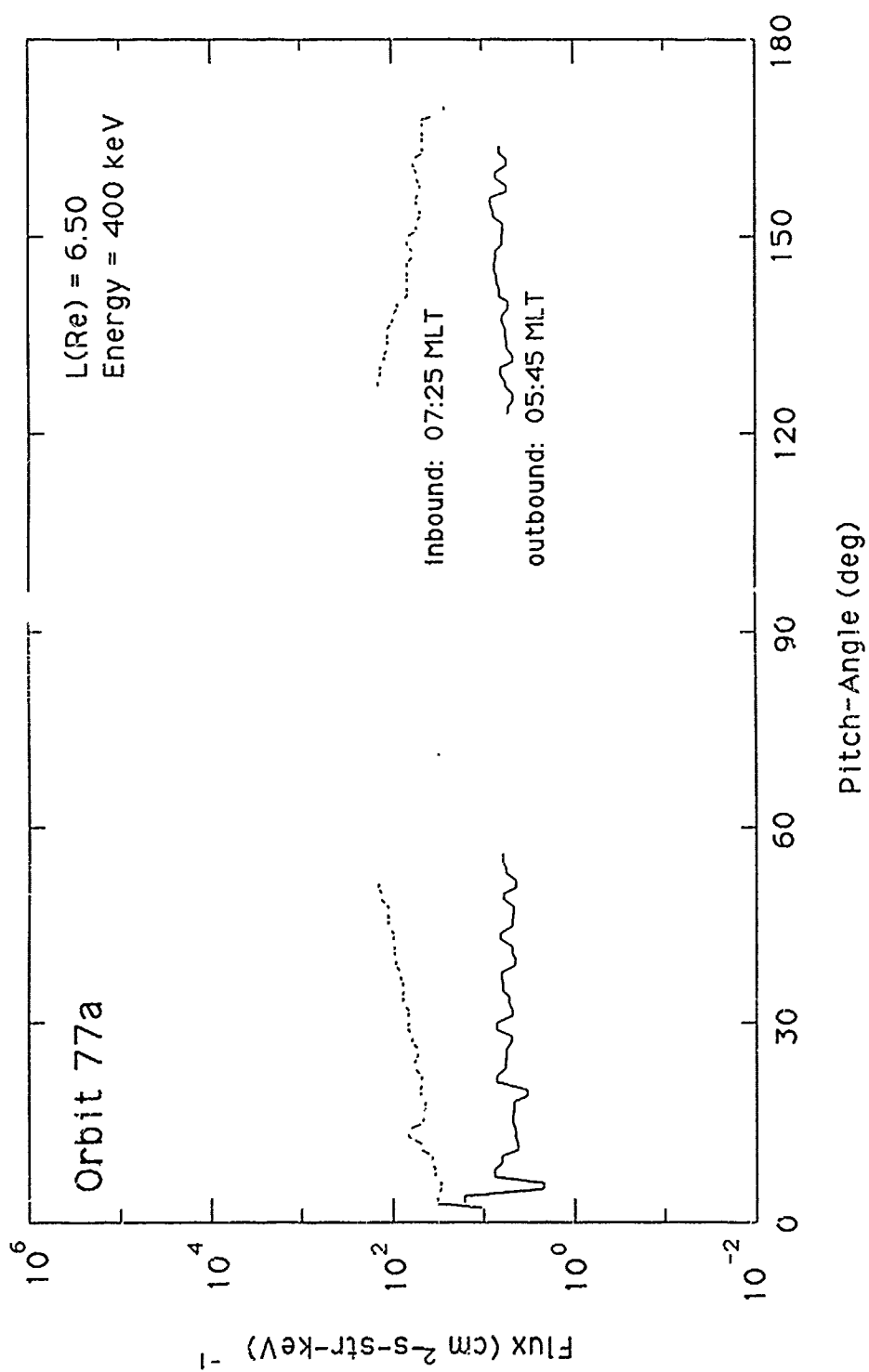


Figure 12

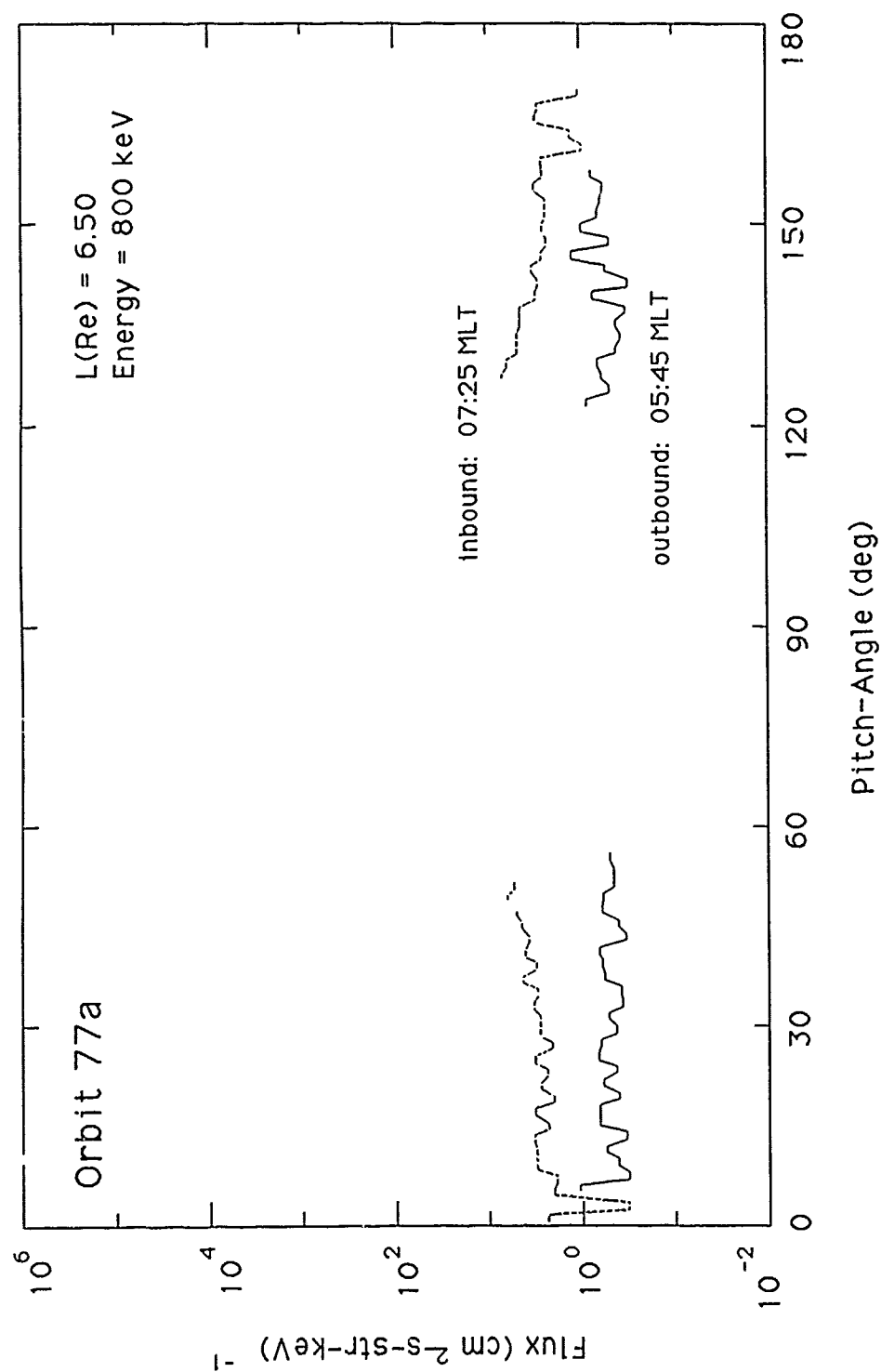


Figure 13

A. Energy Spectrum Before Dropout

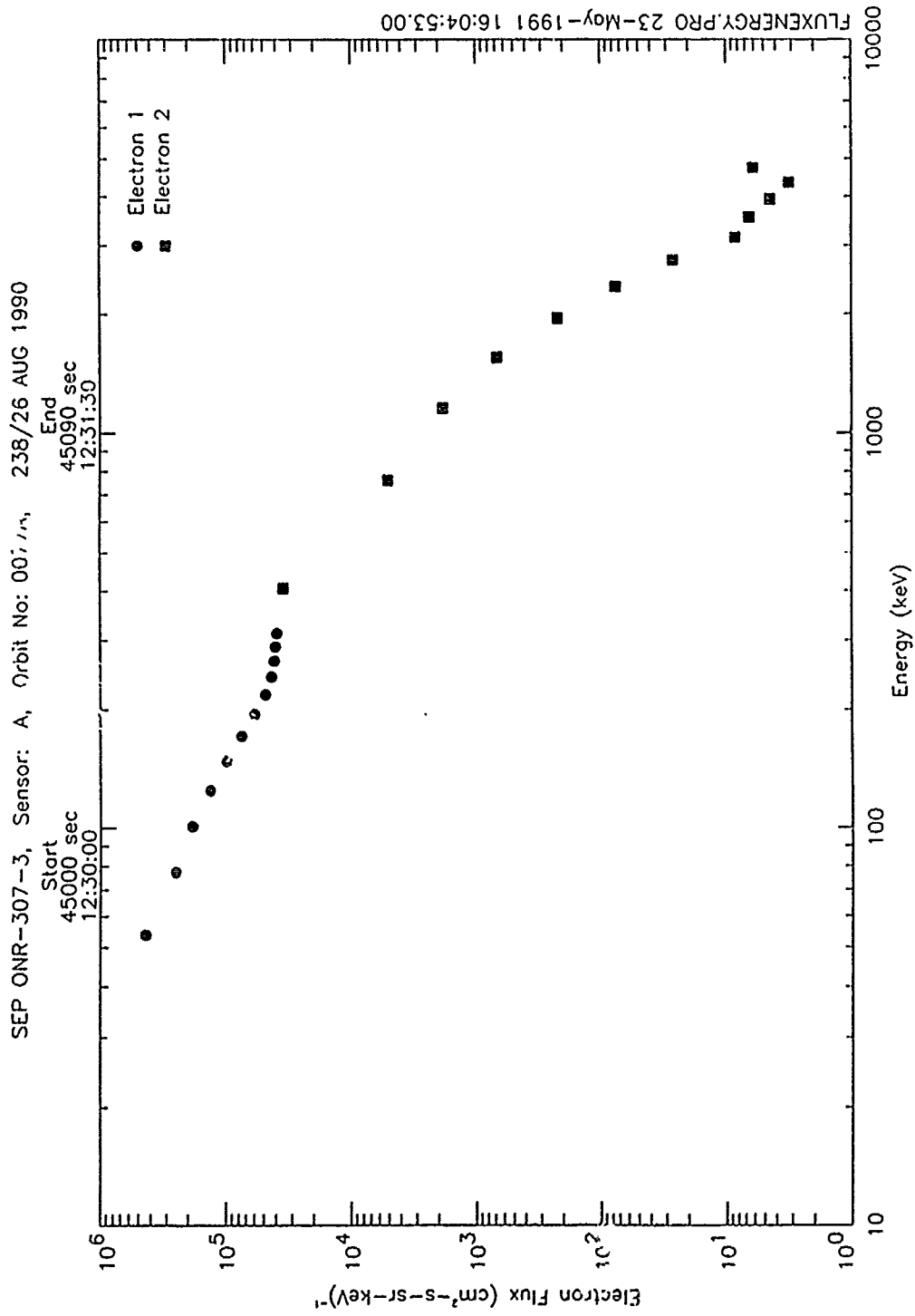


Figure 14

B. Energy Spectrum During Dropout

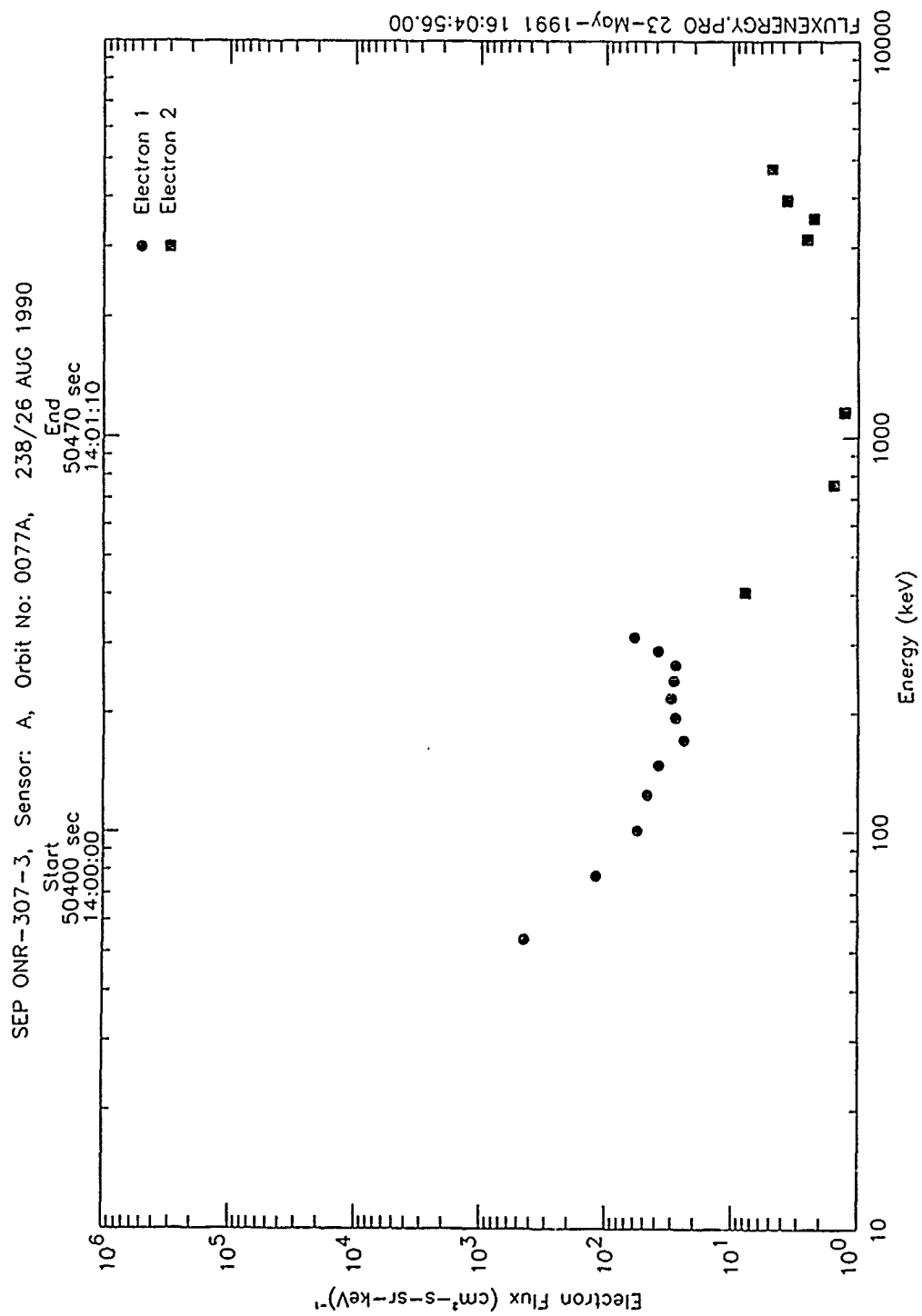


Figure 15

C. Energy Spectrum After Dropout

SEP ONR-307-3, Sensor: A, Orbit No: 0077A, 238/26 AUG 1990

Start
57600 sec
16:00:00

End
57670 sec
16:01:10

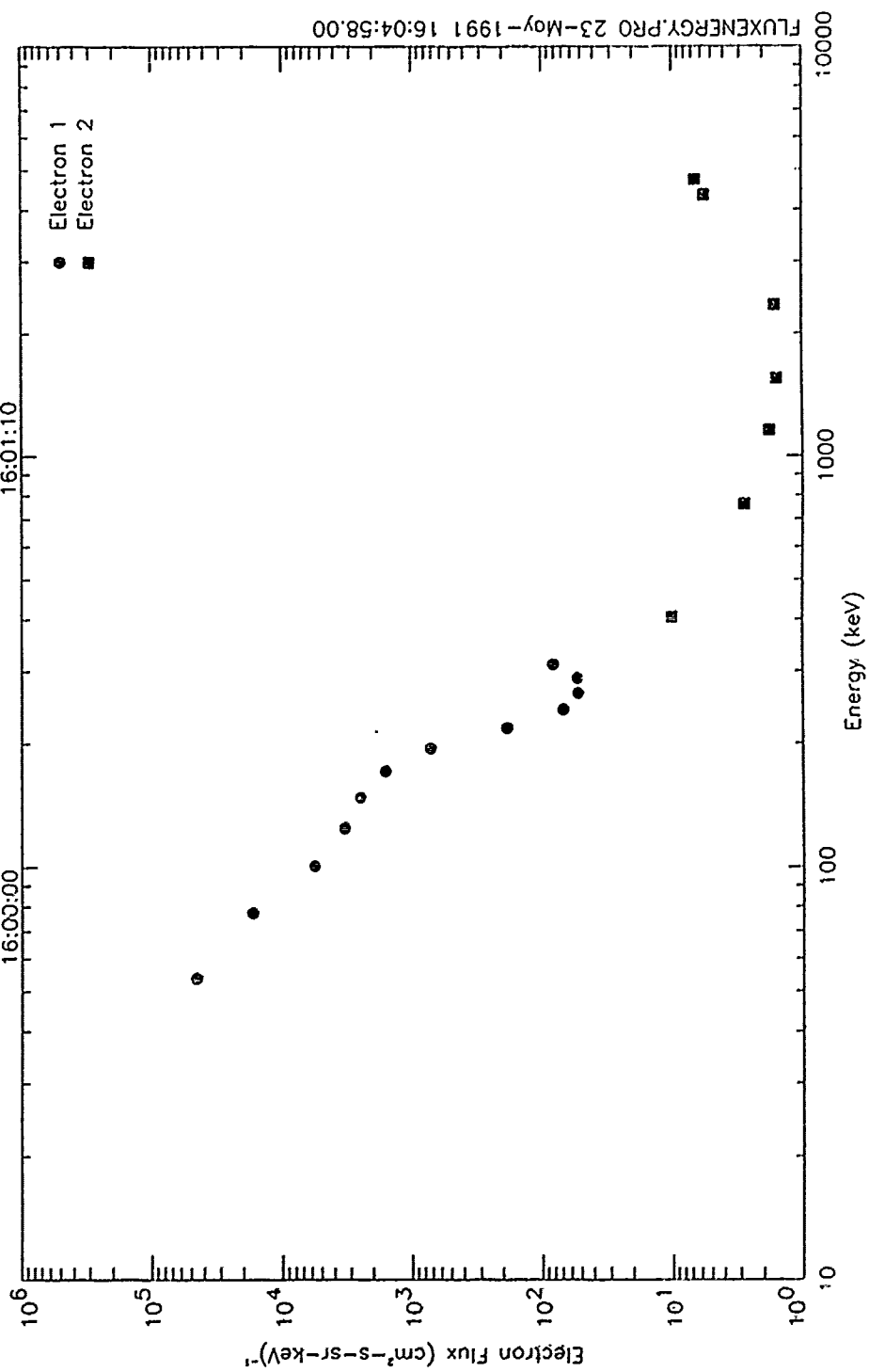


Figure 16

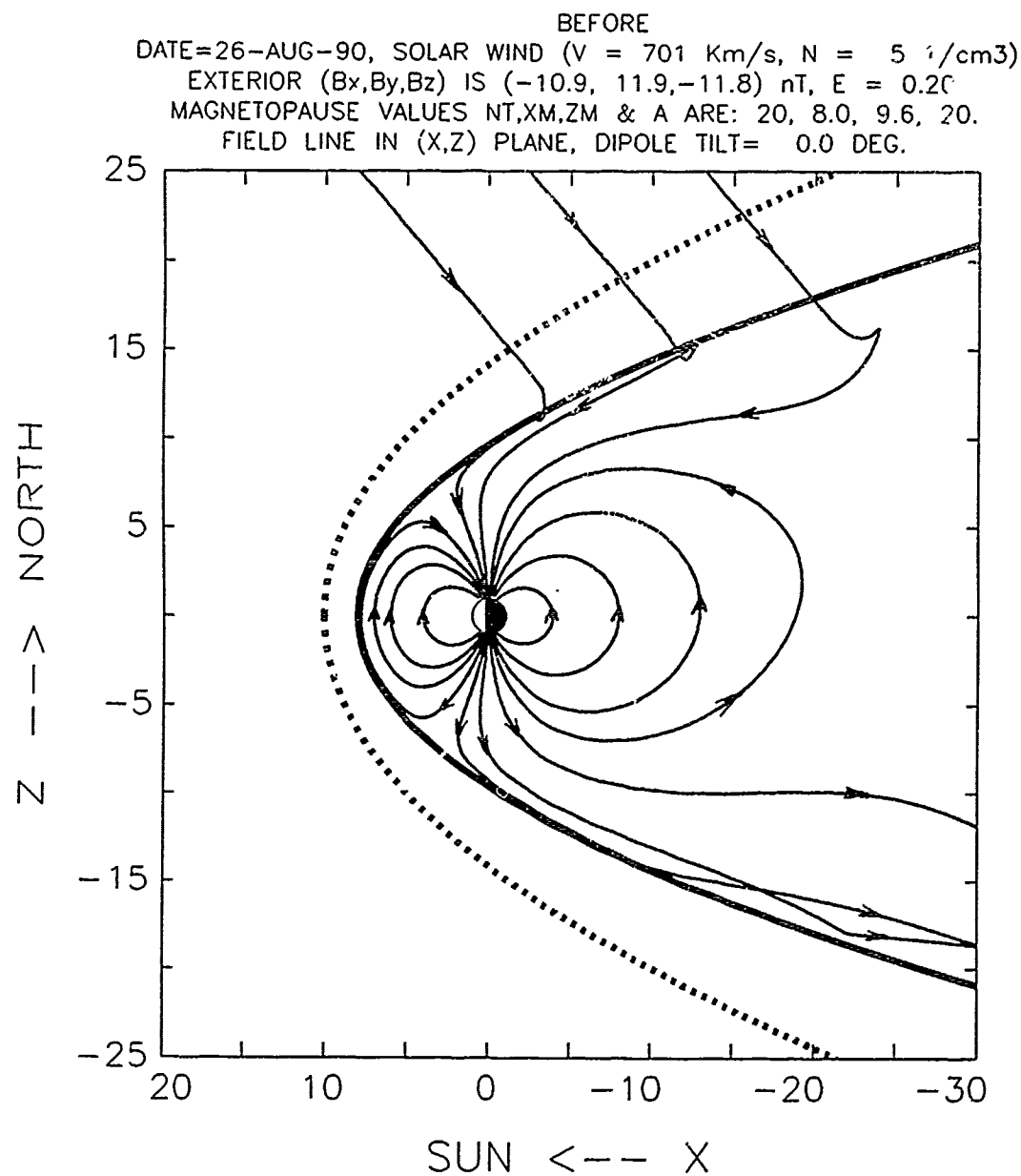


Figure 17

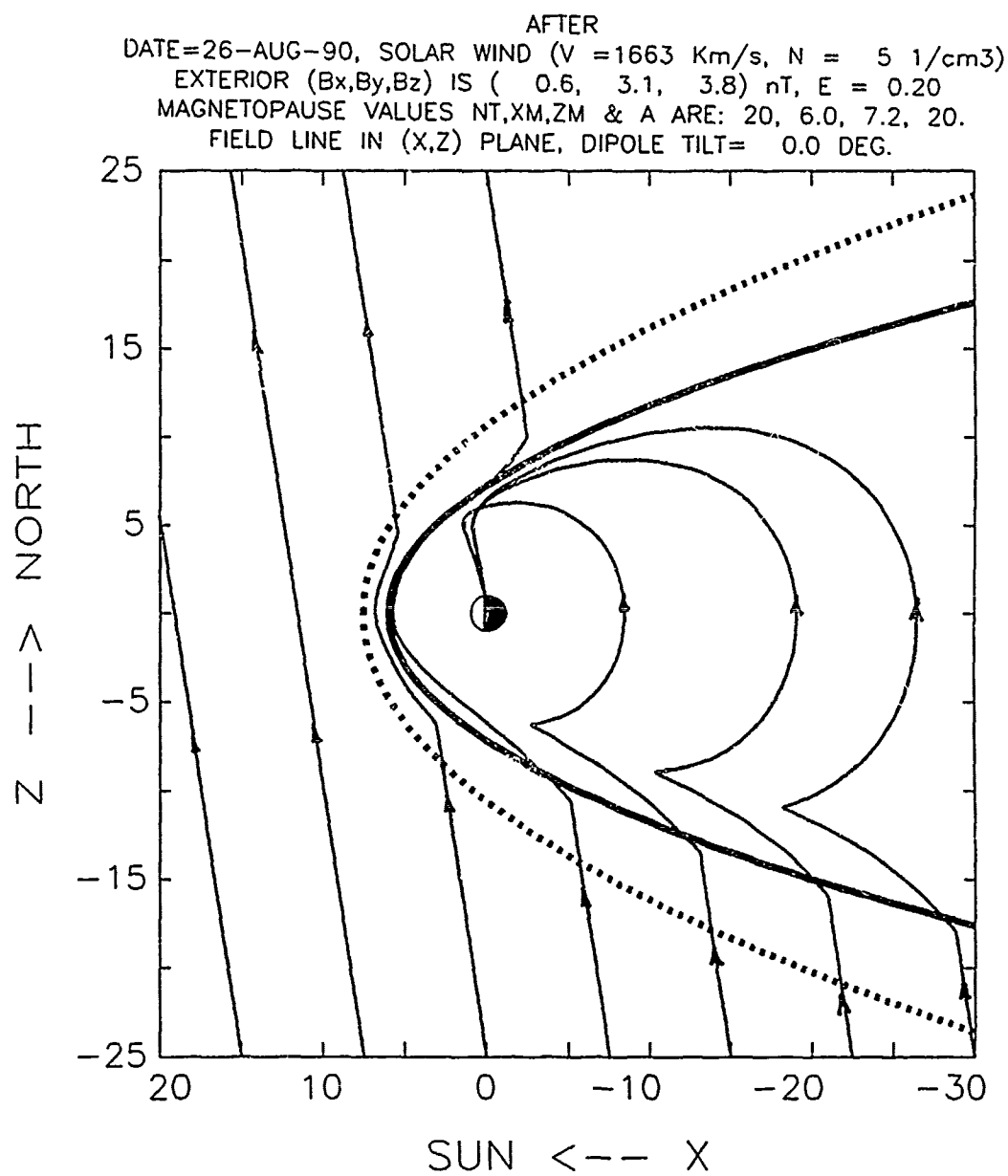


Figure 18

BOW SHOCK & OPEN MAGNETOPAUSE FIELD LINE TRACE
 DATE=26-FEB-91, SOLAR WIND ($V = 1663$ Km/s, $N = 5$ 1/cm³)
 EXTERIOR (B_x, B_y, B_z) IS (0.6, 3.1, 3.8) nT, $E = 0.20$
 MAGNETOPAUSE VALUES NT, X_M, Z_M & A ARE: 20, 6.0, 7.2, 20.
 FIELD LINE IN (X,Y) PLANE, DIPOLE TILT= 0.0 DEG.

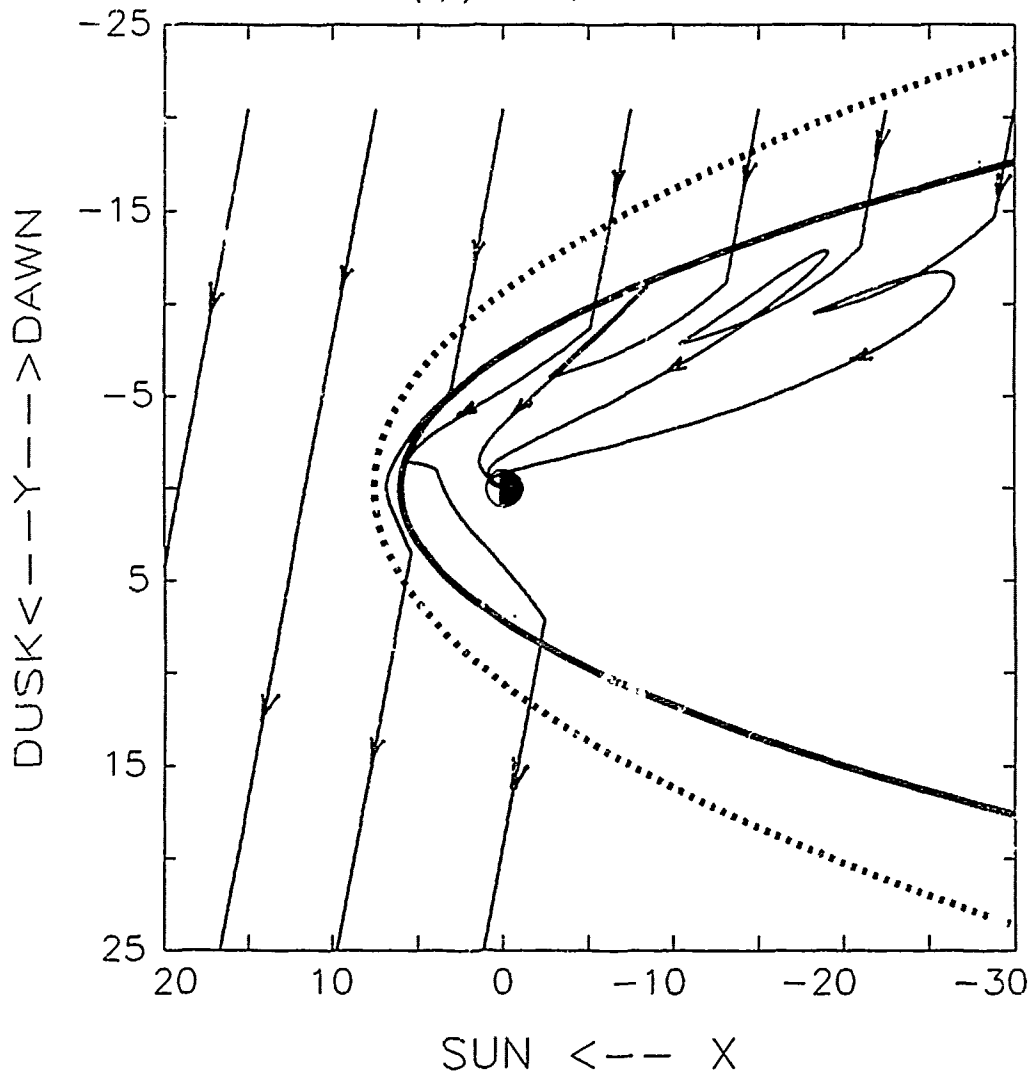


Figure 19

BOW SHOCK & OPEN MAGNETOPAUSE FIELD LINE TRACE
 DATE=26-FEB-91, SOLAR WIND ($V = 1663$ Km/s, $N = 5$ 1/cm³)
 EXTERIOR (B_x, B_y, B_z) IS (0.6, 3.1, 3.8) nT, $E = 0.20$
 MAGNETOPAUSE VALUES N_T, X_M, Z_M & A ARE: 20, 6.0, 7.2, 20.
 FIELD LINE IN (Y,Z) PLANE, DIPOLE TILT= 0.0 DEG.

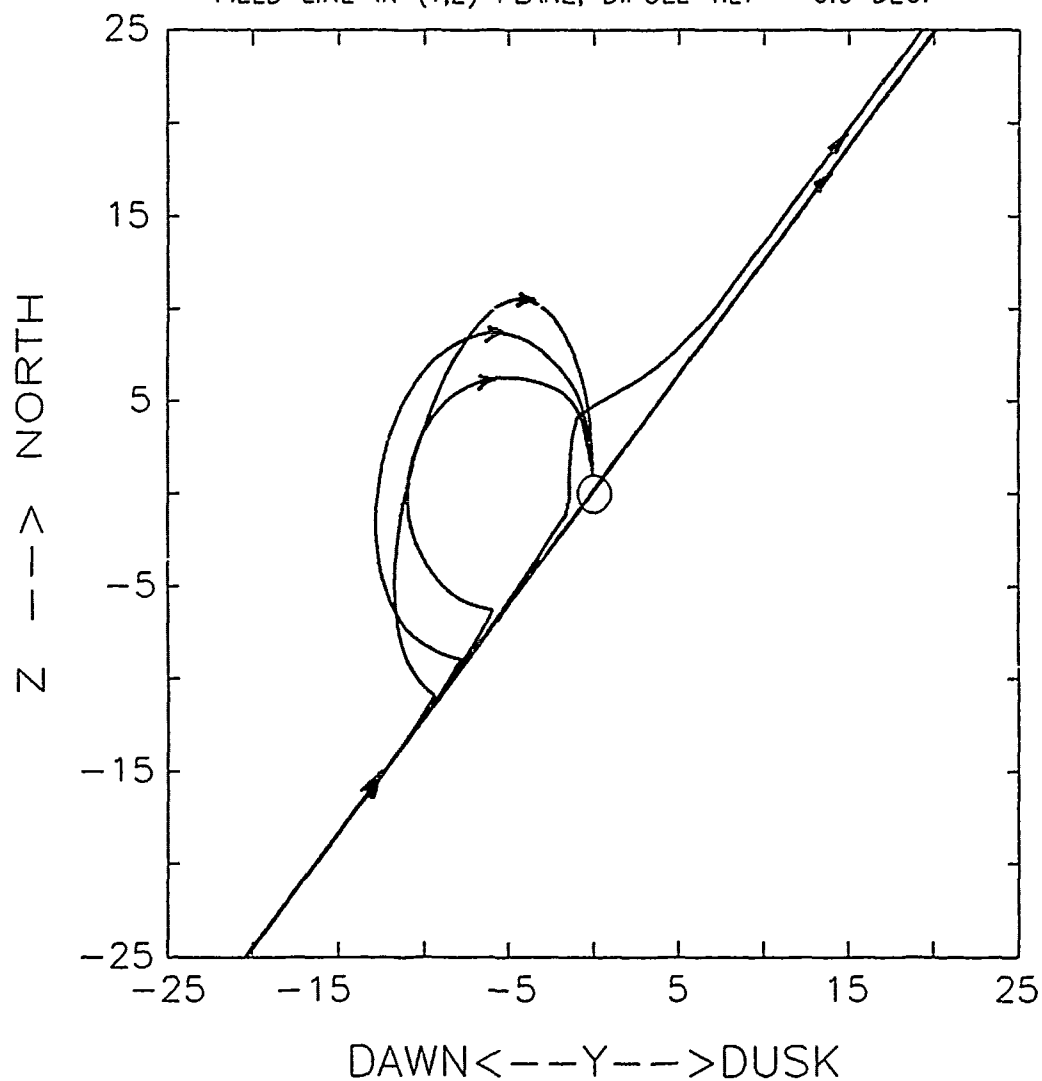


Figure 20

(DEPT. 91-20), LPARL PARTICLE TRAJECTORY CODE
 STARTED AT (1.6, 0.0, -4.0), P.A. = 90.2 deg
 DATE=14-FEB-91, SOLAR WIND (V= 701 km/s, N= 5 1/cm³)
 EXTERIOR (B_x,B_y,B_z) IS (-10.9, 11.9,-11.8) nT, E= 0.20
 B_{ext}=20.02-[1.+0.00*SIN(1.0*PHI+ 0.)+0.00*SIN(1.0*PHI+ 0.)]
 MAGNETOPAUSE BOUNDARY VALUES X_M & Y_M=Z_M ARE: 8.0, 9.6
 ELECTRON, Q=-1, ENERGY=10.004 Mev
 TRAJECTORY ON (X,Y) PLANE, DIPOLE TILT= 0.0 DEG.

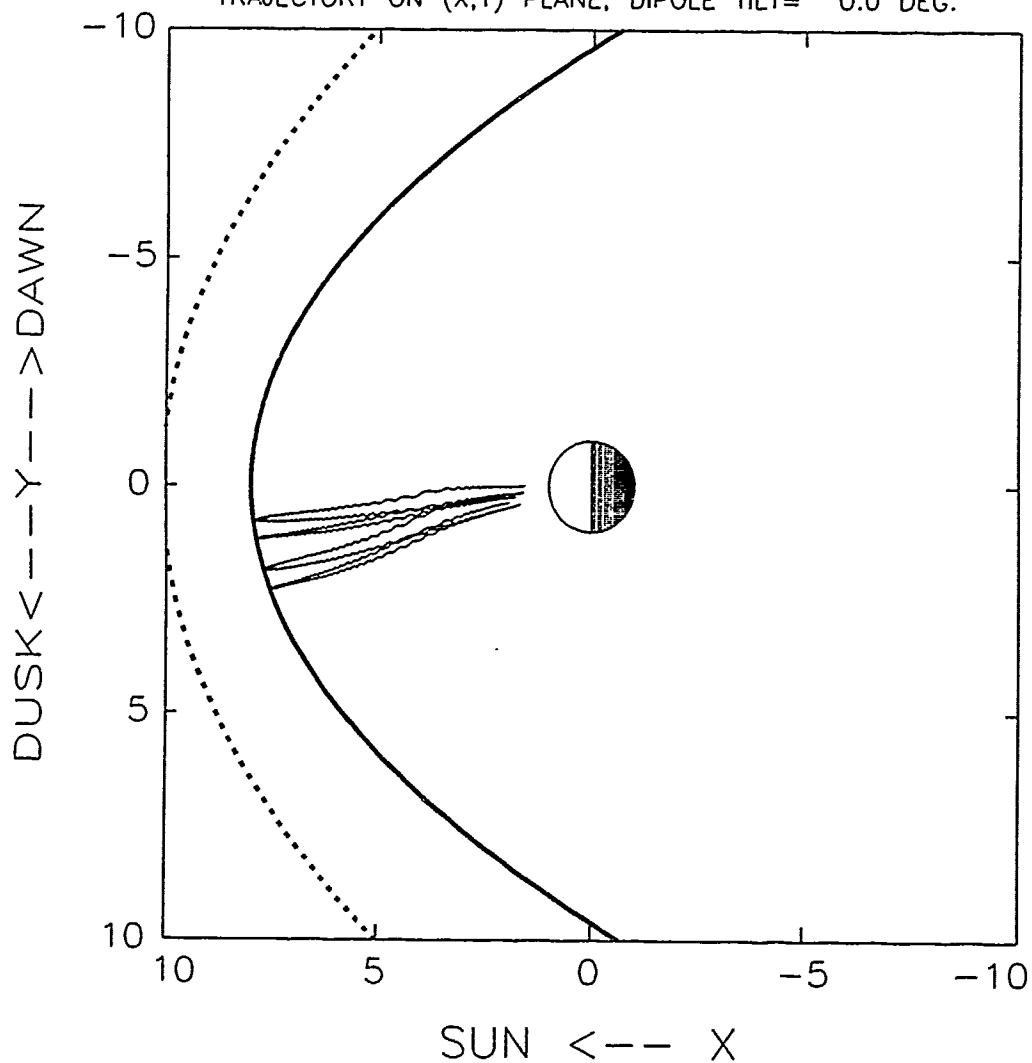


Figure 21

(DEPT. 91-20), LPARL PARTICLE TRAJECTORY CODE
 STARTED AT (1.6, 0.0, -4.0), P.A. = 90.2 deg
 DATE=14-FEB-91, SOLAR WIND (V= 701 km/s, N= 5 1/cm³)
 EXTERIOR (B_x,B_y,B_z) IS (-10.9, 11.9,-11.8) nT, E= 0.20
 $B_{ext}=20.02*[1.+0.00*\sin(1.0*PHI+0.)+0.00*\sin(1.0*PHI+0.)]$
 MAGNETOPAUSE BOUNDARY VALUES X_M & Y_M=Z_M ARE: 8.0, 9.6
 ELECTRON, Q=-1, ENERGY=10.004 Mev
 TRAJECTORY ON (X,Z) PLANE, DIPOLE TILT= 0.0 DEG.

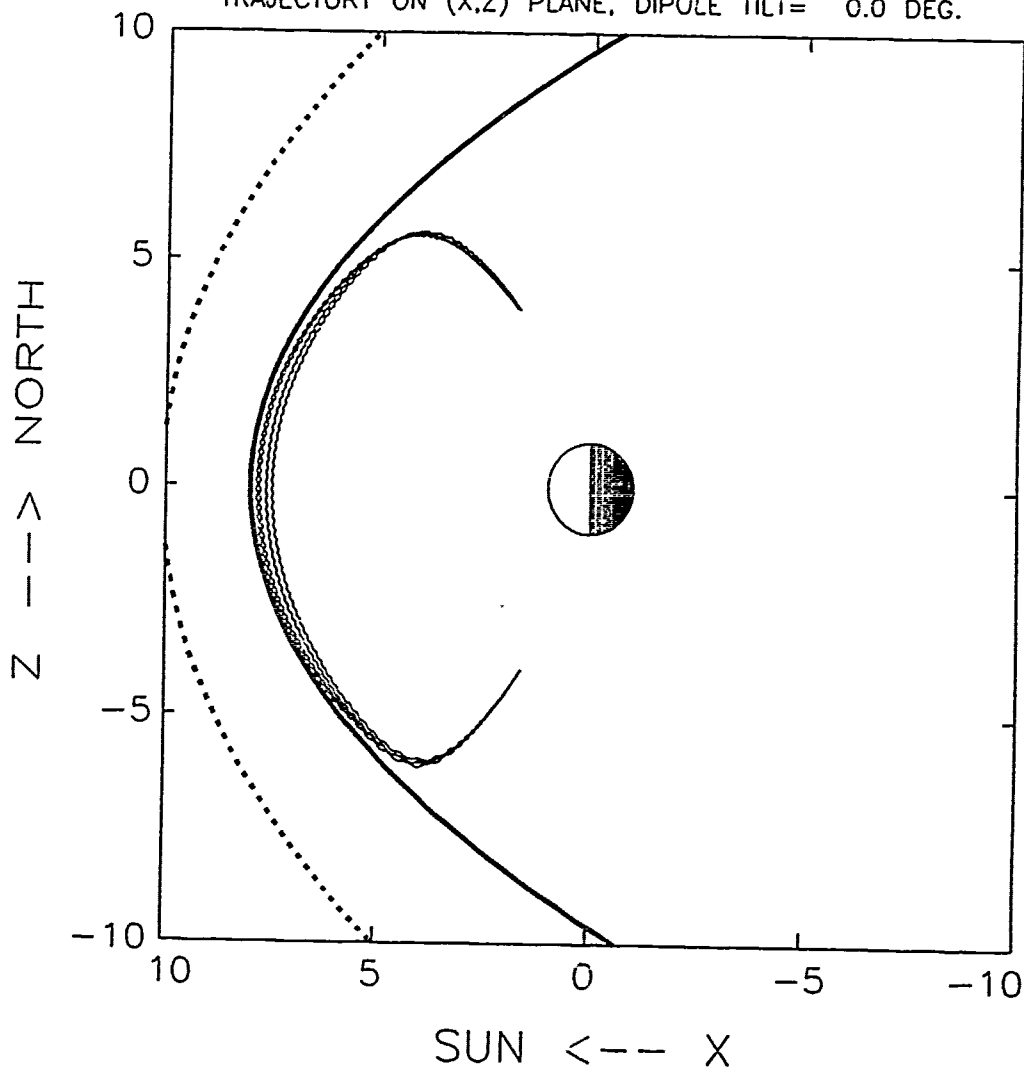


Figure 22

(DEPT. 91-20), LPARL PARTICLE TRAJECTORY CODE
 STARTED AT (1.6, 0.0, -4.0), P.A. = 90.2 deg
 DATE=14-FEB-91, SOLAR WIND (V= 701 km/s, N= 5 1/cm³)
 EXTERIOR (Bx,By,Bz) IS (-10.9, 11.9,-11.8) nT, \bar{E} = 0.20
 $B_{ext}=20.02*[1.+0.00*\sin(1.0*PHI+ 0.)+0.00*\sin(1.0*PHI+ G.)]$
 MAGNETOPAUSE BOUNDARY VALUES XM & YM=ZM ARE: 8.0, 9.6
 ELECTRON, Q=-1, ENERGY=10.004 Mev
 TRAJECTORY ON (Y,Z) PLANE, DIPOLE TILT= 0.0 DEG.

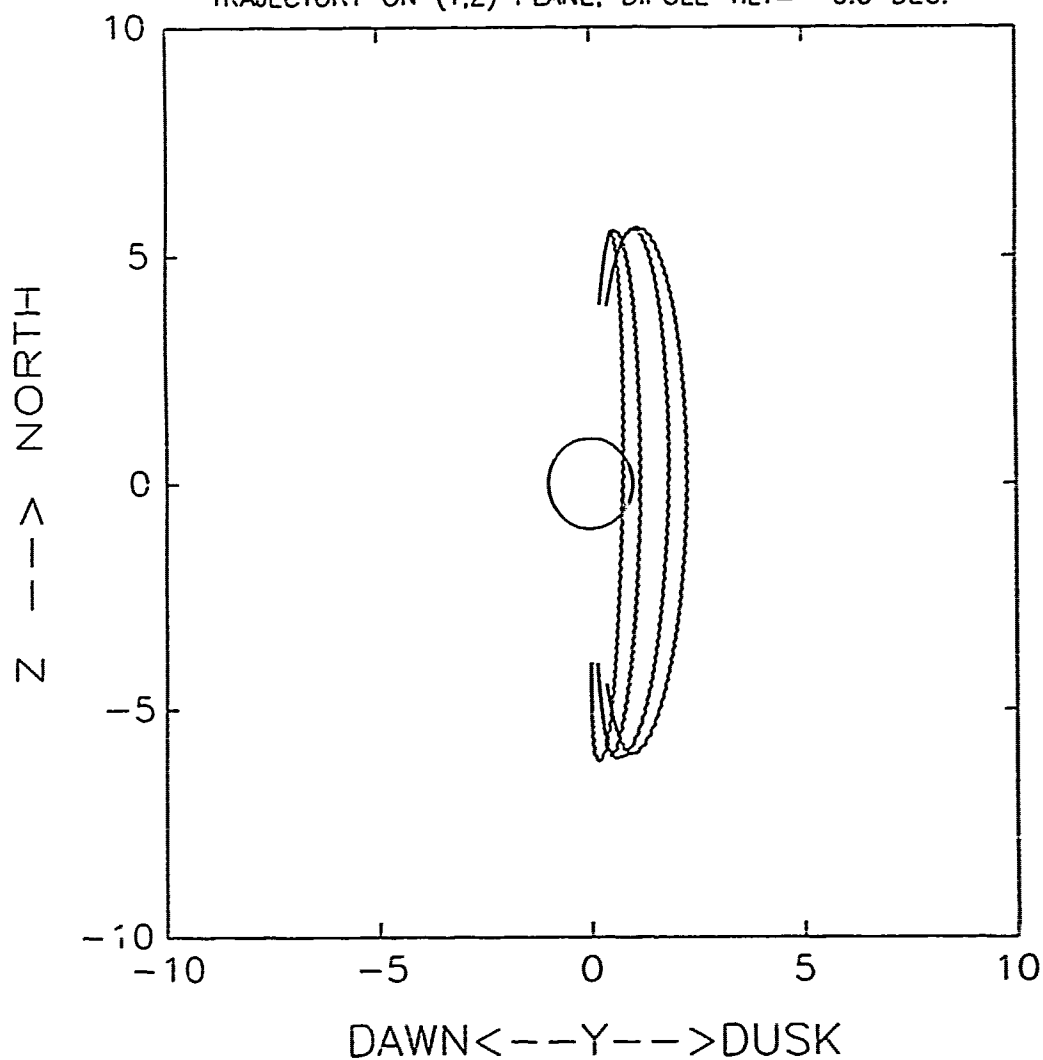


Figure 23

(DEPT. 91-20), LPARL PARTICLE TRAJECTORY CODE
 STARTED AT (1.6, 0.0, -4.0), P.A. = 90.1 deg
 DATE=14-FEB-91, SOLAR WIND (V=1663 km/s, N= 5 1/cm³)
 EXTERIOR (B_x,B_y,B_z) IS (0.6, 3.1, 3.8) nT, E= 0.20
 $B_{ext} = 5.00 * [1.0 + 0.00 * \sin(1.0 * \phi + 0.0) + 0.00 * \sin(1.0 * \phi + 0.0)]$
 MAGNETOPAUSE BOUNDARY VALUES X_M & Y_M=Z_M ARE: 6.0, 7.2
 ELECTRON, Q=-1, ENERGY=10.004 Mev
 TRAJECTORY ON (X,Y) PLANE, DIPOLE TILT= 0.0 DEG.

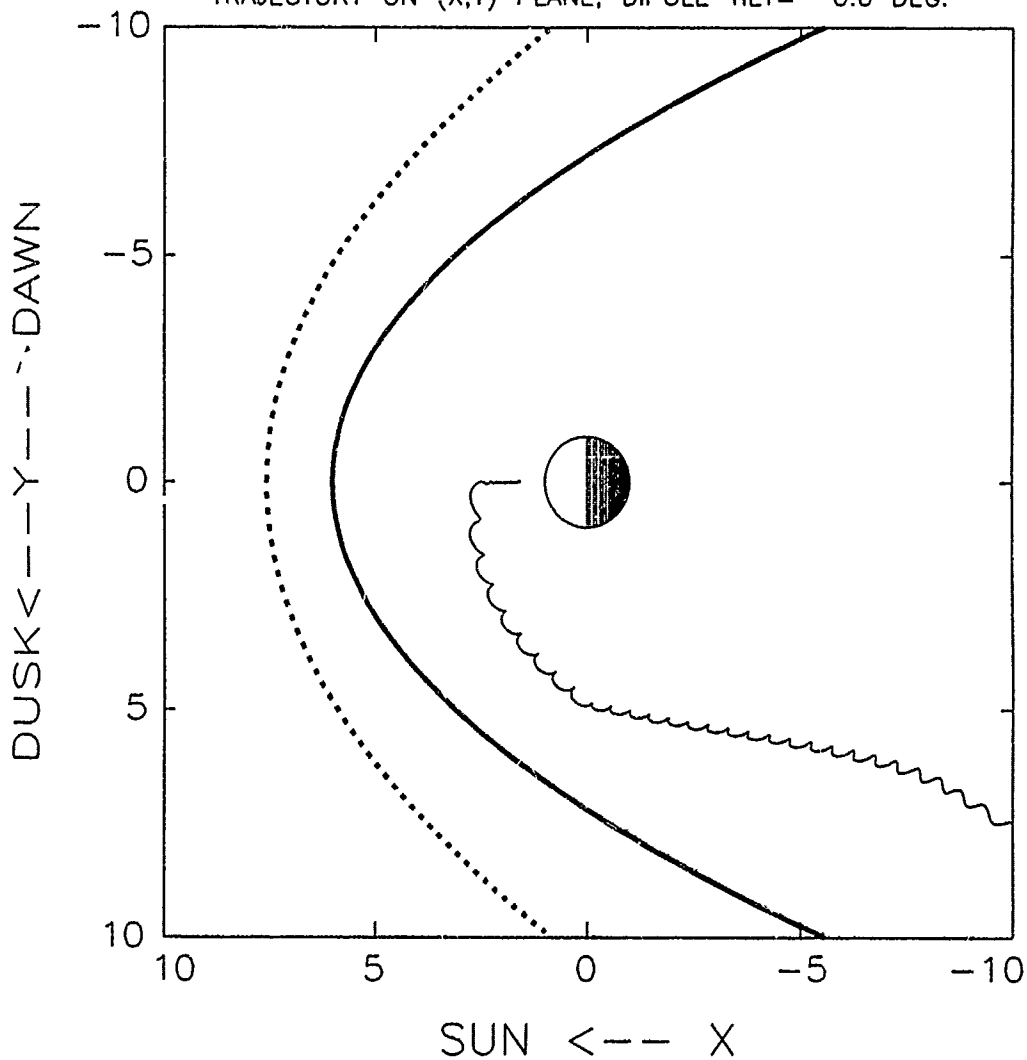


Figure 24

(DEPT. 91-20), LPARL PARTICLE TRAJECTORY CODE
 STARTED AT (1.6, 0.0, -4.0), P.A. = 90.1 deg
 DATE=14-FEB-91, SOLAR WIND ($V=1663$ km/s, $N= 5$ 1/cm³)
 EXTERIOR (B_x, B_y, B_z) IS (0.6, 3.1, 3.8) nT, $E= 0.20$
 $B_{ext} = 5.00 * [1.0 + 0.00 * \sin(1.0 * \theta_{HI} + 0.0) + 0.00 * \sin(1.0 * \theta_{HI} + 0.0)]$
 MAGNETOPAUSE BOUNDARY VALUES X_M & $Y_M = Z_M$ ARE: 6.0, 7.2
 ELECTRON, $Q=-1$, ENERGY=10.004 MeV
 TRAJECTORY ON (X,Z) PLANE, DIPOLE TILT= 0.0 DEG.

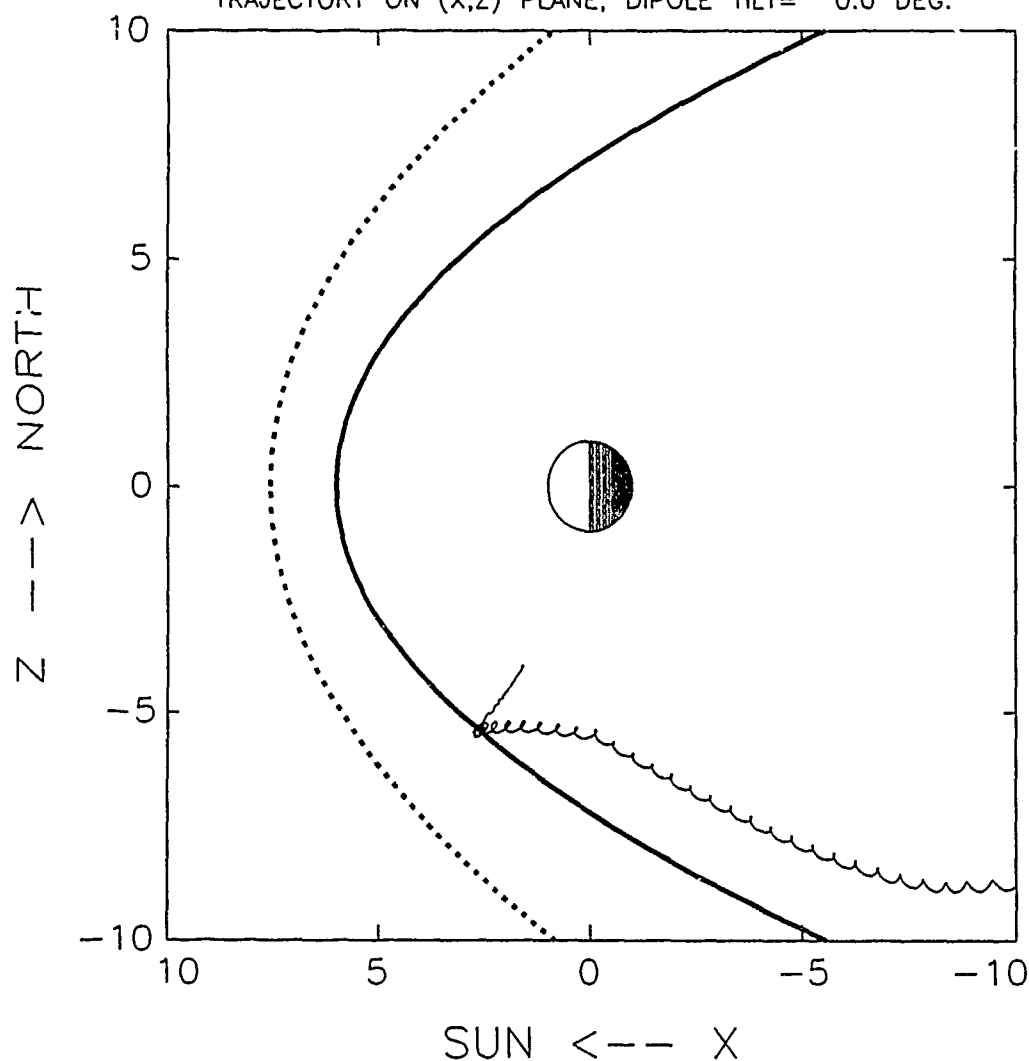


Figure 25

(DEPT. 91-20), LPARL PARTICLE TRAJECTORY CODE
 STARTED AT (1.6, 0.0, -4.0), P.A. = 90.1 deg
 DATE=14-FEB-91, SOLAR WIND (V=1663 km/s, N= 5 1/cm³)
 EXTERIOR (B_x,B_y,B_z) IS (0.6, 3.1, 3.8) nT, E= 0.20
 B_{ext}= 5.00*[1.0+0.00*SIN(1.0*PHI+ 0.0)+0.00*SIN(1.0*PHI+ 0.0)]
 MAGNETOPAUSE BOUNDARY VALUES X_M & Y_M=Z_M ARE: 6.0, 7.2
 ELECTRON, Q=-1, ENERGY=10.004 Mev
 TRAJECTORY ON (Y,Z) PLANE, DIPOLE TILT= 0.0 DEG.

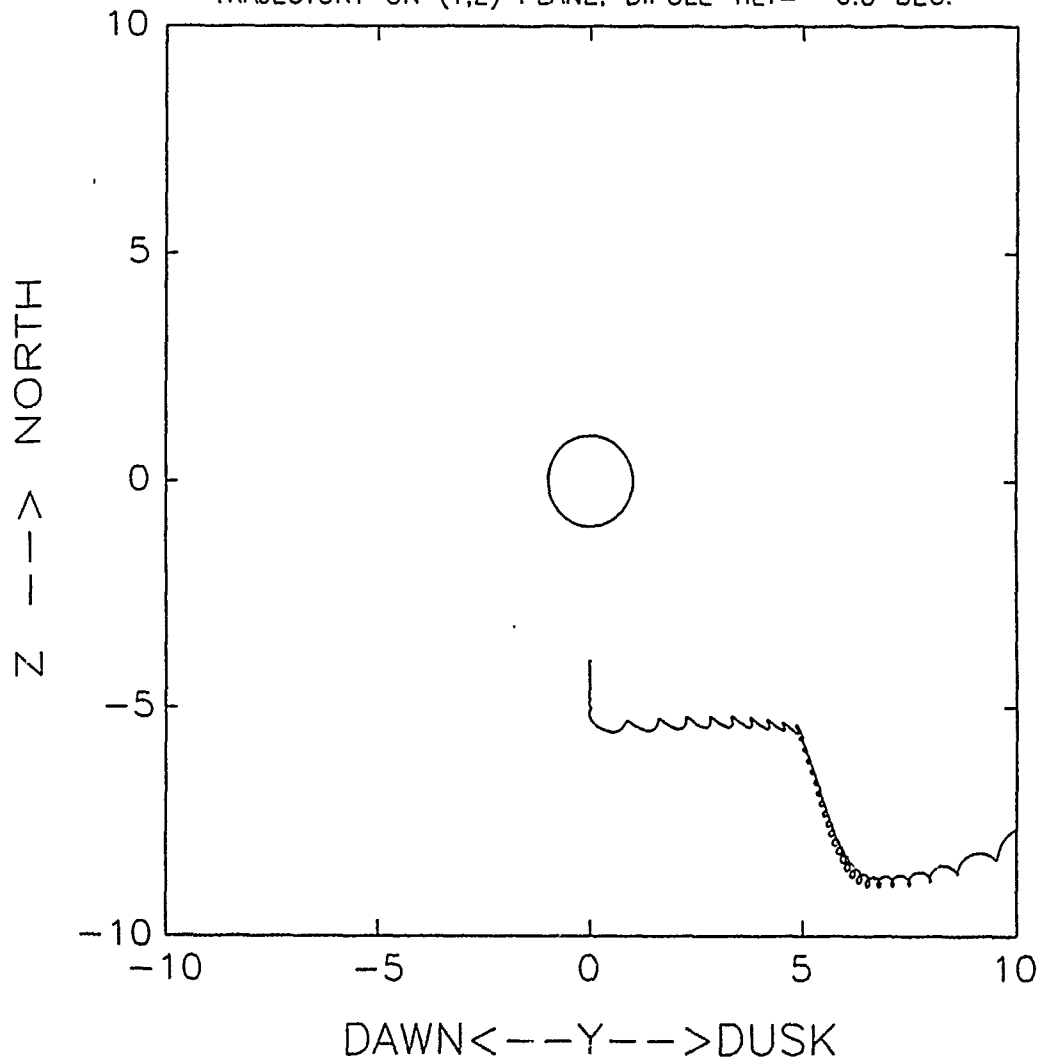


Figure 26

(DEPT. 91-20), LPARL PARTICLE TRAJECTORY CODE
 STARTED AT (1.0, -6.3, 0.0), P.A. = 90.8 deg
 DATE=15-FEB-91, SOLAR WIND (V= 701 km/s, N= 5 1/cm³)
 EXTERIOR (B_x,B_y,B_z) IS (-10.9, 11.9,-11.8) nT, E= 0.20
 Bext=20.02*[1.+0.00*SIN(1.0*PHI+ 0.)+0.00*SIN(1.0*PHI+ 0.)]
 MAGNETOPAUSE BOUNDARY VALUES XM & YM=ZM ARE: 8.0, 9.6
 ELECTRON, Q=-1, ENERGY=10.004 Mev
 TRAJECTORY ON (X,Y) PLANE, DIPOLE TILT= 0.0 DEG.

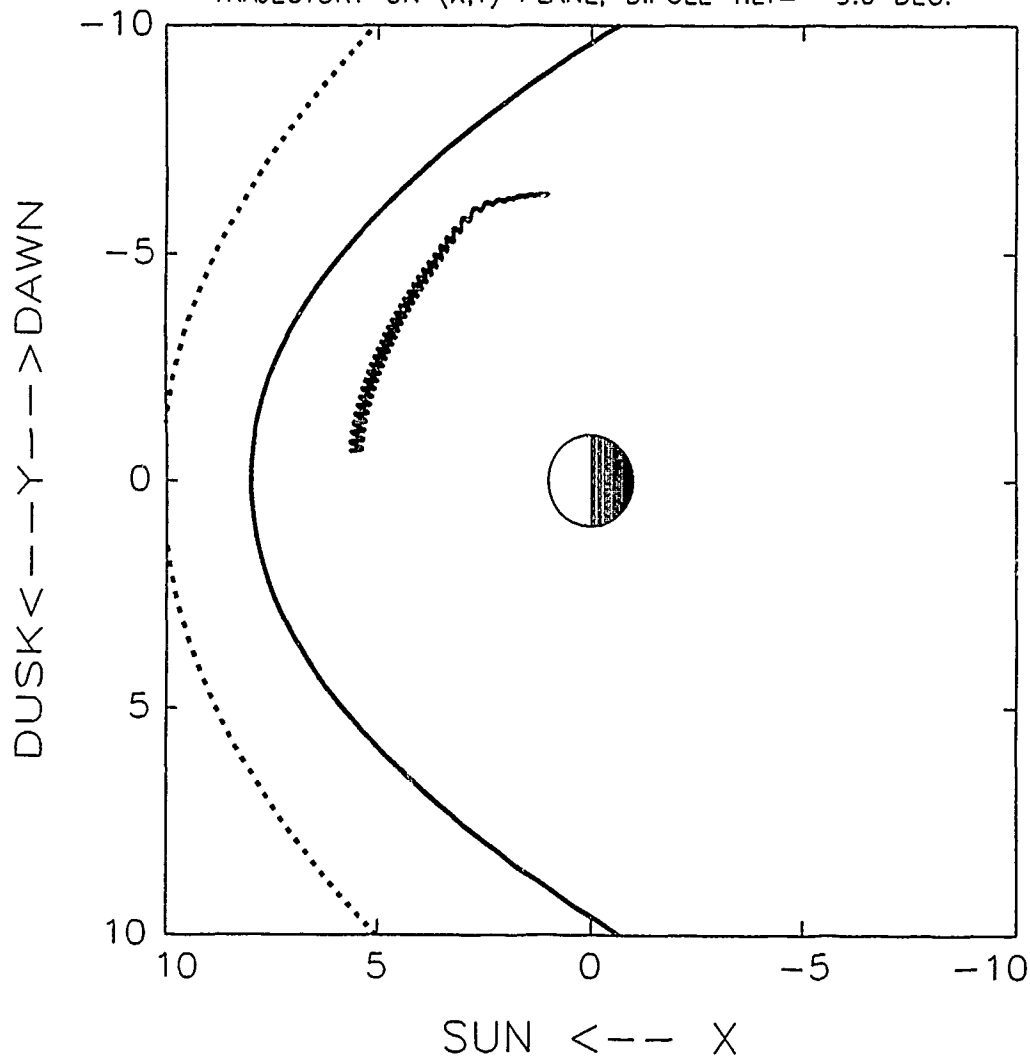


Figure 27

(DEPT. 91-20), LPARL PARTICLE TRAJECTORY CODE
 STARTED AT (1.0, -6.3, 0.0), P.A. = 90.8 deg
 DATE=15-FEB-91, SOLAR WIND (V= 701 km/s, N= 5 1/cm³)
 EXTERIOR (B_x,B_y,B_z) IS (-10.9, 11.9,-11.8) nT, E= 0.20
 $B_{ext}=20.02*[1.0+0.00*\sin(1.0*PHI+0.0)+0.00*\sin(1.0*PHI+0.0)]$
 MAGNETOPAUSE BOUNDARY VALUES X_M & Y_M=Z_M ARE: 8.0, 9.6
 ELECTRON, Q=-1, ENERGY=10.004 Mev
 TRAJECTORY ON (X,Z) PLANE, DIPOLE TILT= 0.0 DEG.

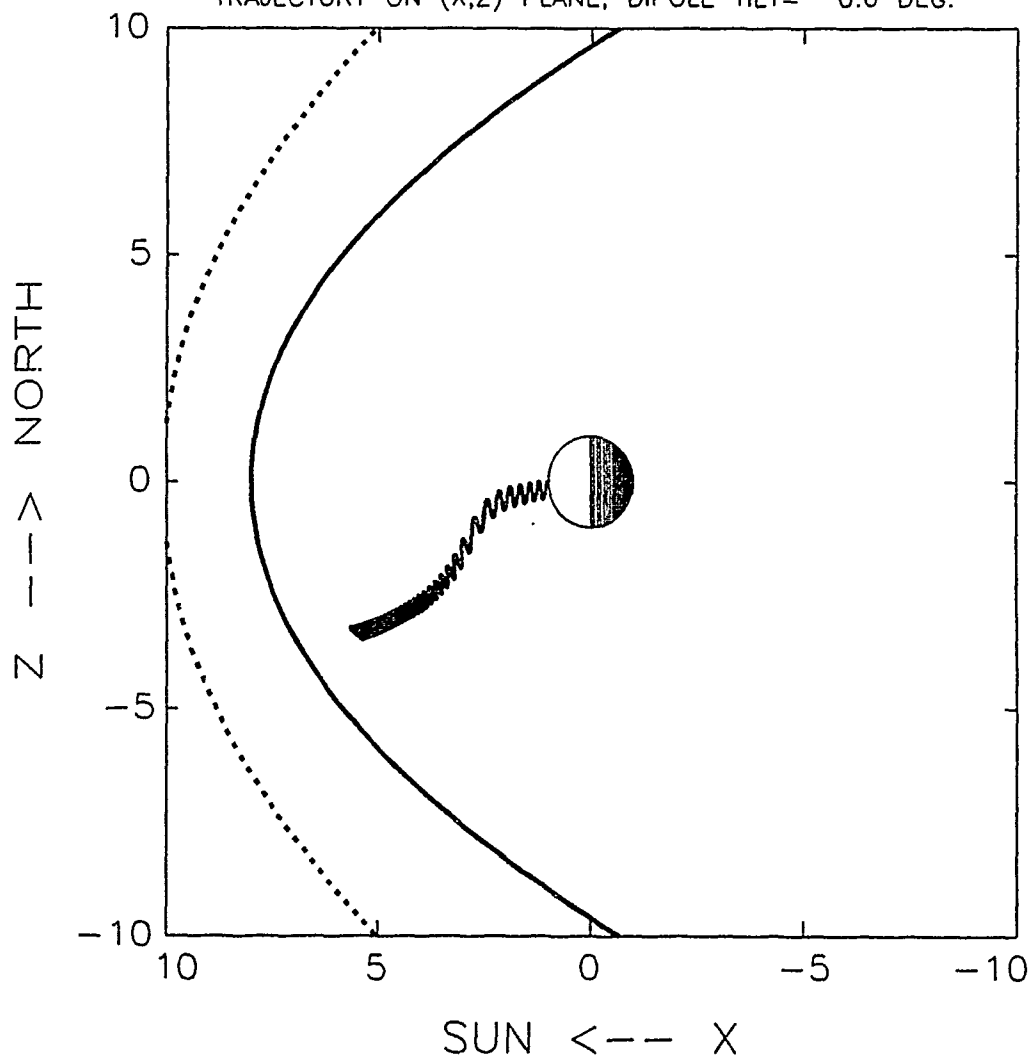


Figure 28

(DEPT. 91-20), LPARL PARTICLE TRAJECTORY CODE
 STARTED AT (1.0, -6.3, 0.0), P.A. = 90.8 deg
 DATE=15-FEB-91, SOLAR WIND (V= 701 km/s, N= 5 1/cm³)
 EXTERIOR (B_x,B_y,B_z) IS (-10.9, 11.9,-11.8) nT, E= 0.20
 B_{ext}=20.02*[1.+0.00*SIN(1.0*PHI+ 0.)+0.00*SIN(1.0*PHI+ 0.)]
 MAGNETOPAUSE BOUNDARY VALUES X_M & Y_M=Z_M ARE: 8.0, 9.6
 ELECTRON, Q=-1, ENERGY=10.004 Mev
 TRAJECTORY ON (Y,Z) PLANE, DIPOLE TILT= 0.0 DEG.

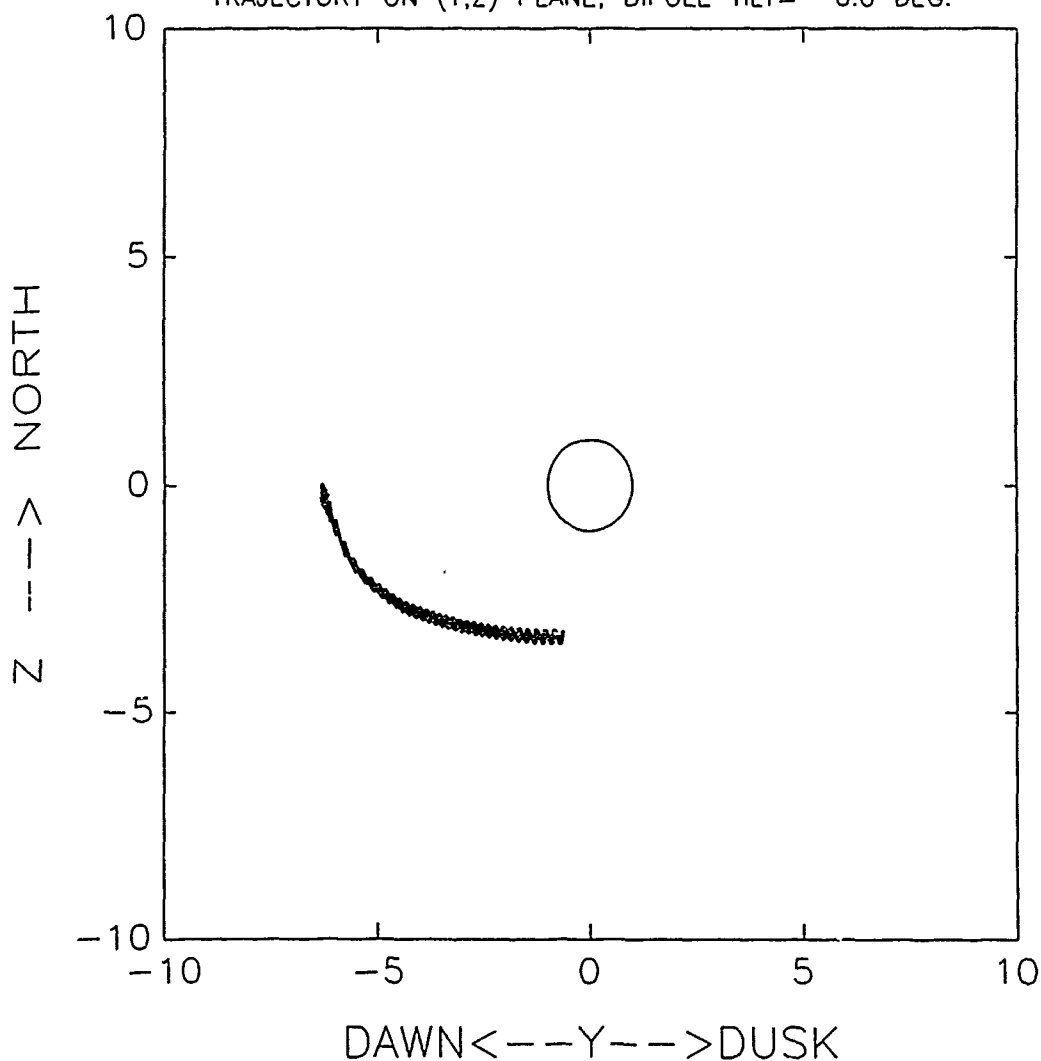


Figure 29

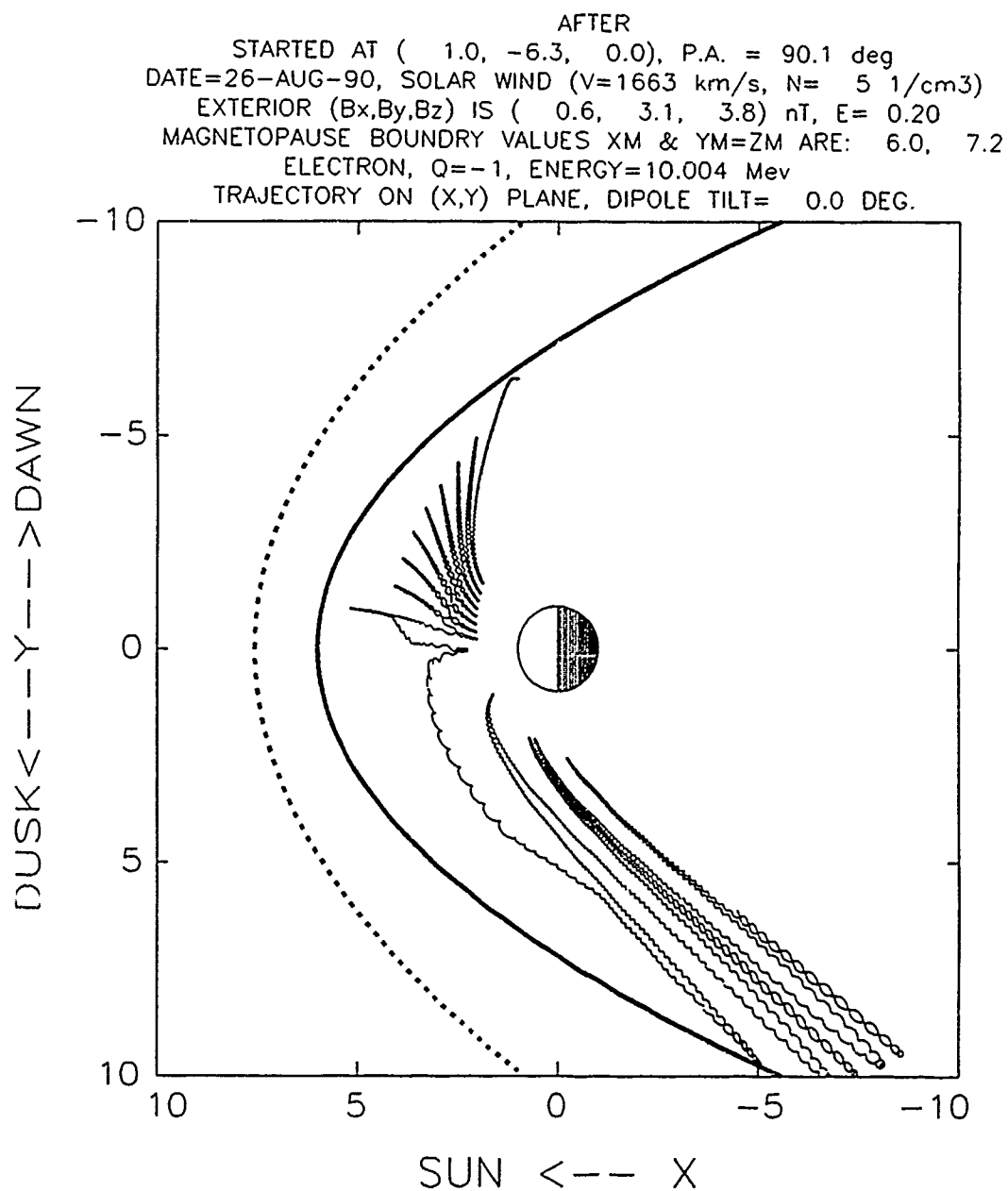


Figure 30

(DEPT. 91-20), LPARL PARTICLE TRAJECTORY CODE
 STARTED AT (1.0, -6.3, 0.0), P.A. = 90.1 deg
 DATE=15-FEB-91, SOLAR WIND (V=1663 km/s, N= 5 1/cm³)
 EXTERIOR (B_x,B_y,B_z) IS (0.6, 3.1, 3.8) nT, E= 0.20
 B_{ext}= 5.00*[1.+0.00*SIN(1.0*PHI+ 0.)+0.00*SIN(1.0*PHI+ 0.)]
 MAGNETOPAUSE BOUNDARY VALUES X_M & Y_M=Z_M ARE: 6.0, 7.2
 ELECTRON, Q=-1, ENERGY=10.004 Mev
 TRAJECTORY ON (X,Z) PLANE, DIPOLE TILT= 0.0 DEG.

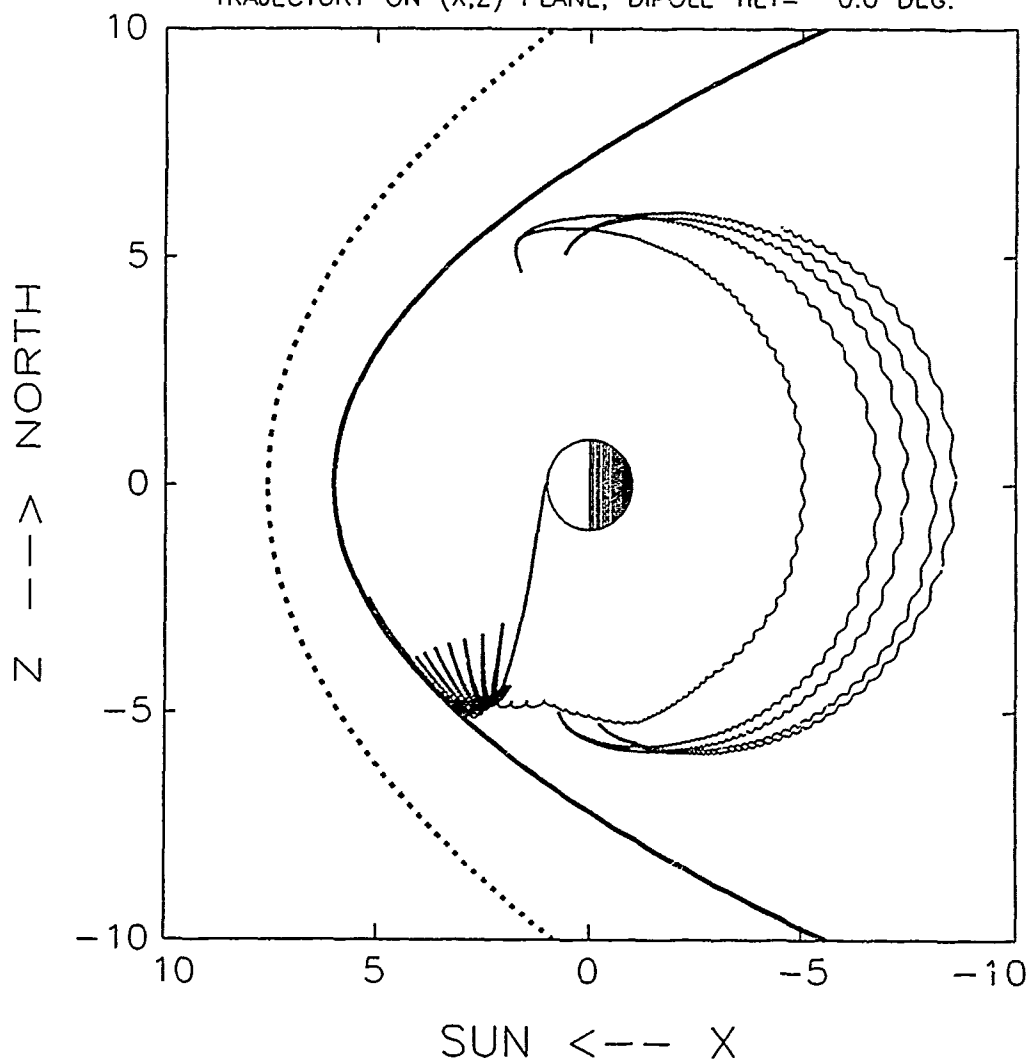


Figure 31

(DEPT. 91-20), LPARL PARTICLE TRAJECTORY CODE
 STARTED AT (1.0, -6.3, 0.0), P.A. = 90.1 deg
 DATE=15-FEB-91, SOLAR WIND (V=1663 km/s, N= 5 1/cm³)
 EXTERIOR (B_x,B_y,B_z) IS (0.6, 3.1, 3.8) nT, E= 0.20
 $B_{ext} = 5.00 * [1.0 + 0.00 * \sin(1.0 * \Phi + 0.0) + 0.00 * \sin(1.0 * \Phi + 0.0)]$
 MAGNETOPAUSE BOUNDARY VALUES X_M & Y_M=Z_M ARE: 6.0, 7.2
 ELECTRON, Q=-1, ENERGY=10.004 Mev
 TRAJECTORY ON (Y,Z) PLANE, DIPOLE TILT= 0.0 DEG.

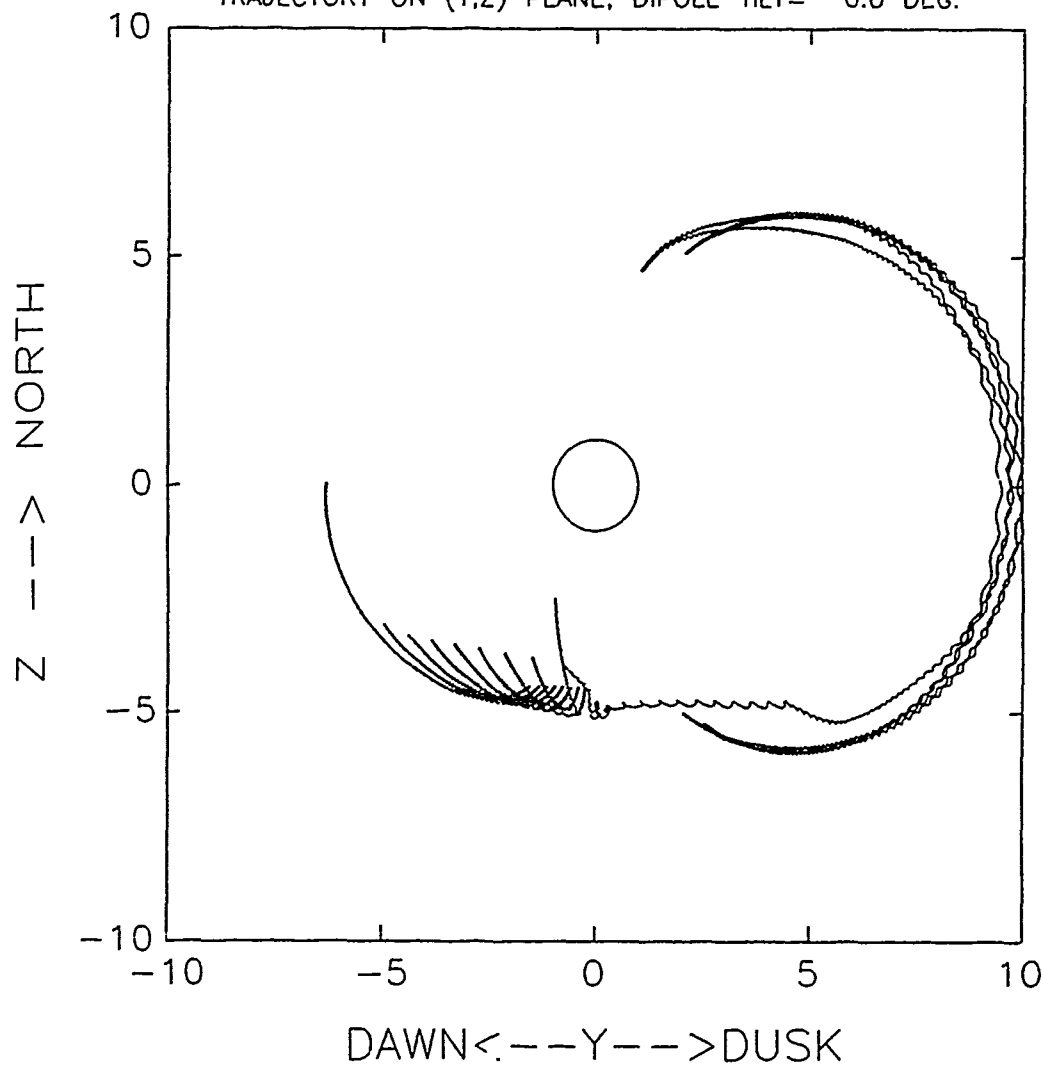


Figure 32

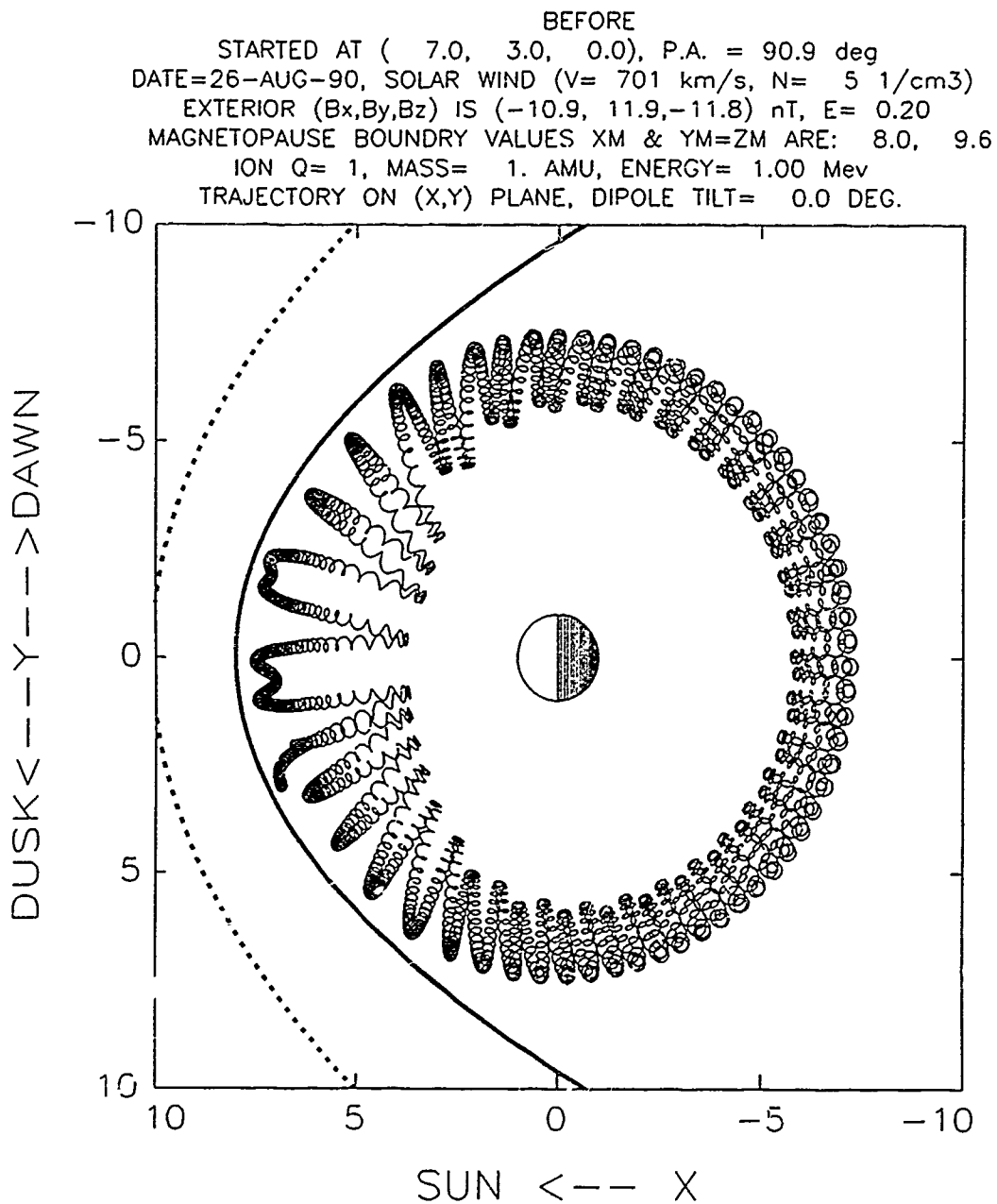


Figure 33

(DEPT. 91-20), LPARL PARTICLE TRAJECTORY CODE
 STARTED AT (7.0, 3.0, 0.0), P.A. = 90.9 deg
 DATE= 8-FEB-91, SOLAR WIND (V= 701 km/s, N= 5 1/cm³)
 EXTERIOR (B_x,B_y,B_z) IS (-10.9, 11.9,-11.8) nT, E= 0.20
 $B_{ext}=20.02*[1.+0.00*\sin(1.0*PHI+0.)+0.00*\sin(1.0*PHI+0.)]$
 MAGNETOPAUSE BOUNDARY VALUES X_M & Y_M=Z_M ARE: 8.0, 9.6
 ION Q= 1, MASS= 1. AMU, ENERGY= 1.00 Mev
 TRAJECTORY ON (X,Z) PLANE, DIPOLE TILT= 0.0 DEG.

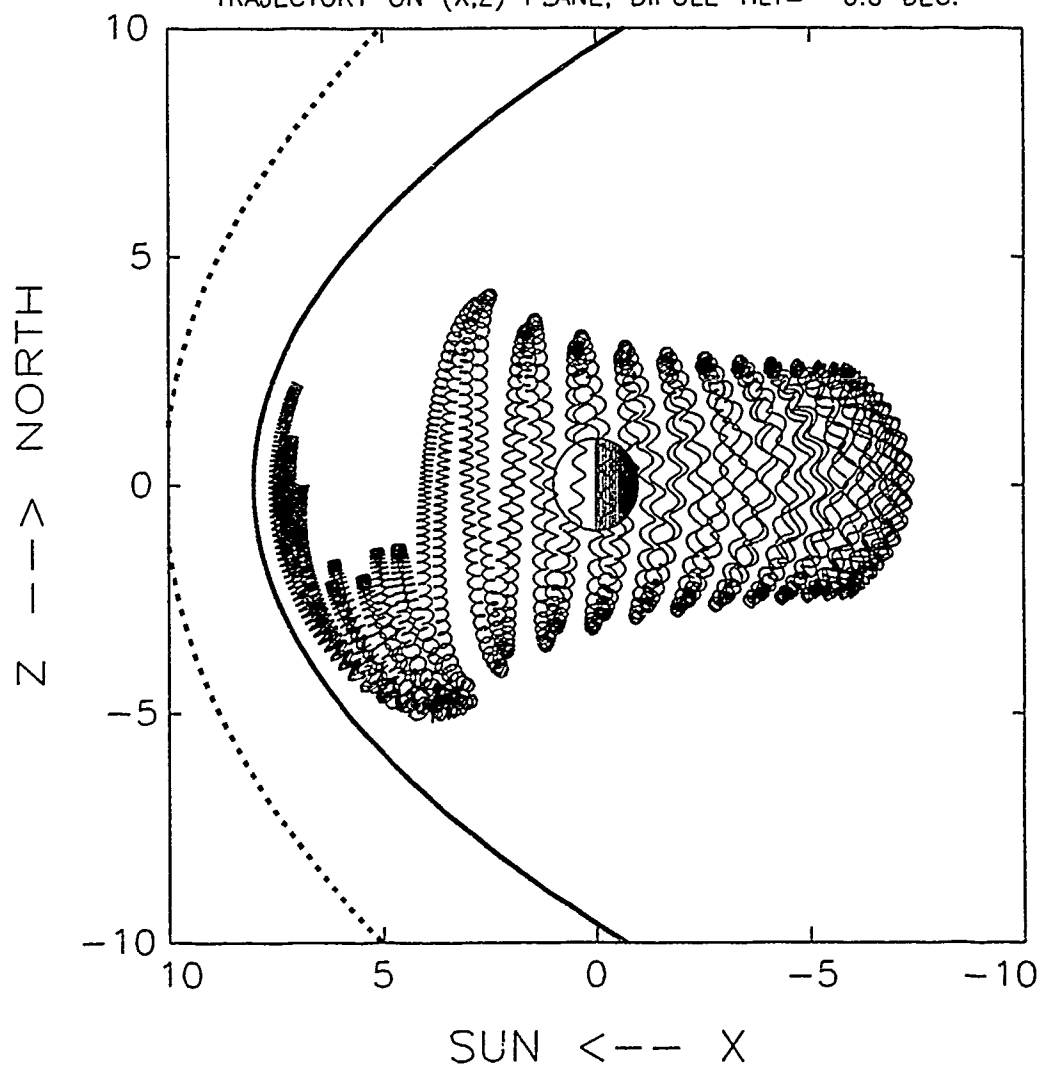


Figure 34

(DEPT. 91-20), LPARL PARTICLE TRAJECTORY CODE
 STARTED AT (7.0, 3.0, 0.0), P.A. = 90.9 deg
 DATE= 8-FEB-91, SOLAR WIND (V= 701 km/s, N= 5 1/cm³)
 EXTERIOR (B_x,B_y,B_z) IS (-10.9, 11.9,-11.8) nT, E= 0.20
 $B_{ext}=20.02*[1.+0.00*\sin(1.0*PHI+0.)+0.00*\sin(1.0*PHI+0.)]$
 MAGNETOPAUSE BOUNDARY VALUES X_M & Y_M=Z_M ARE: 8.0, 9.6
 ION Q= 1, MASS= 1. AMU, ENERGY= 1.00 Mev
 TRAJECTORY ON (Y,Z) PLANE, DIPOLE TILT= 0.0 DEG.

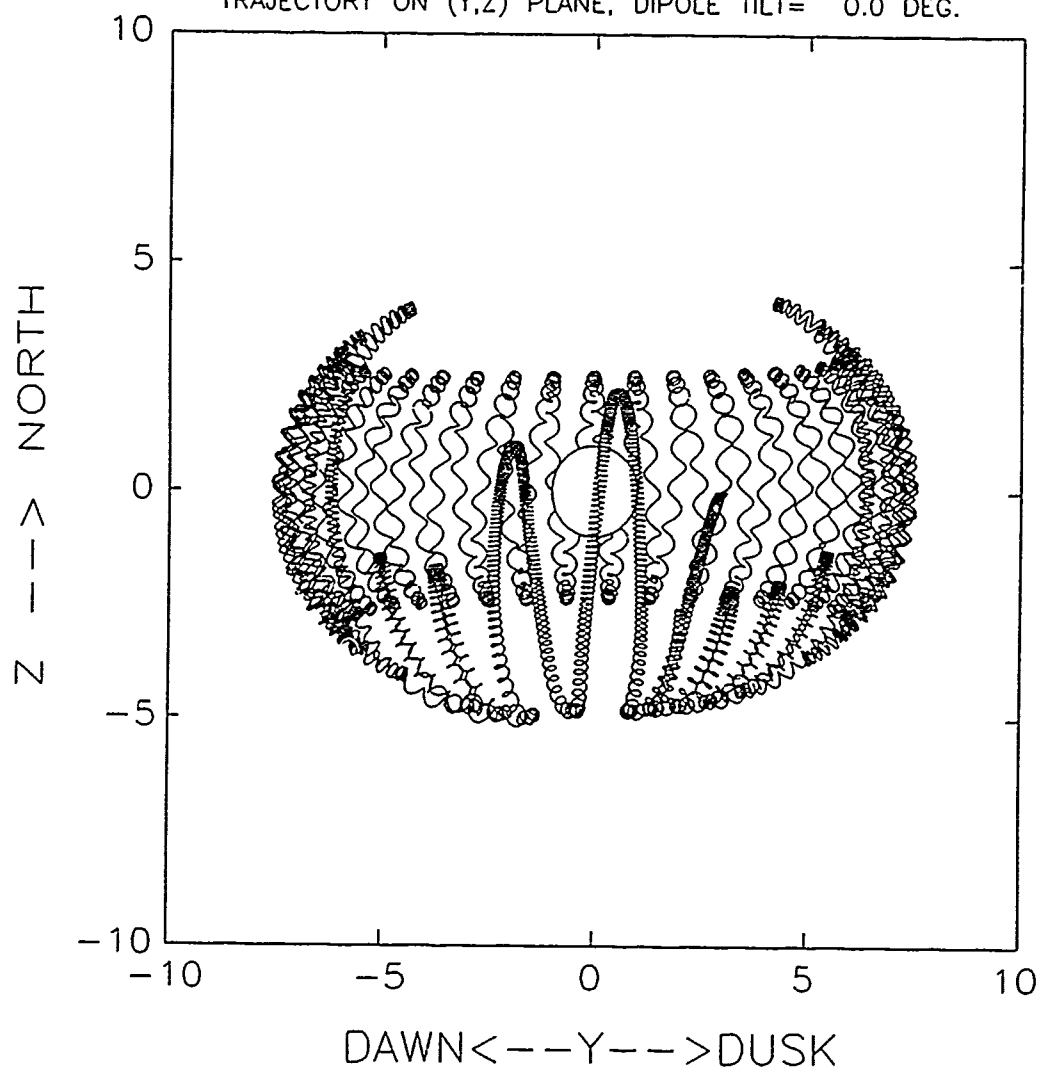


Figure 35

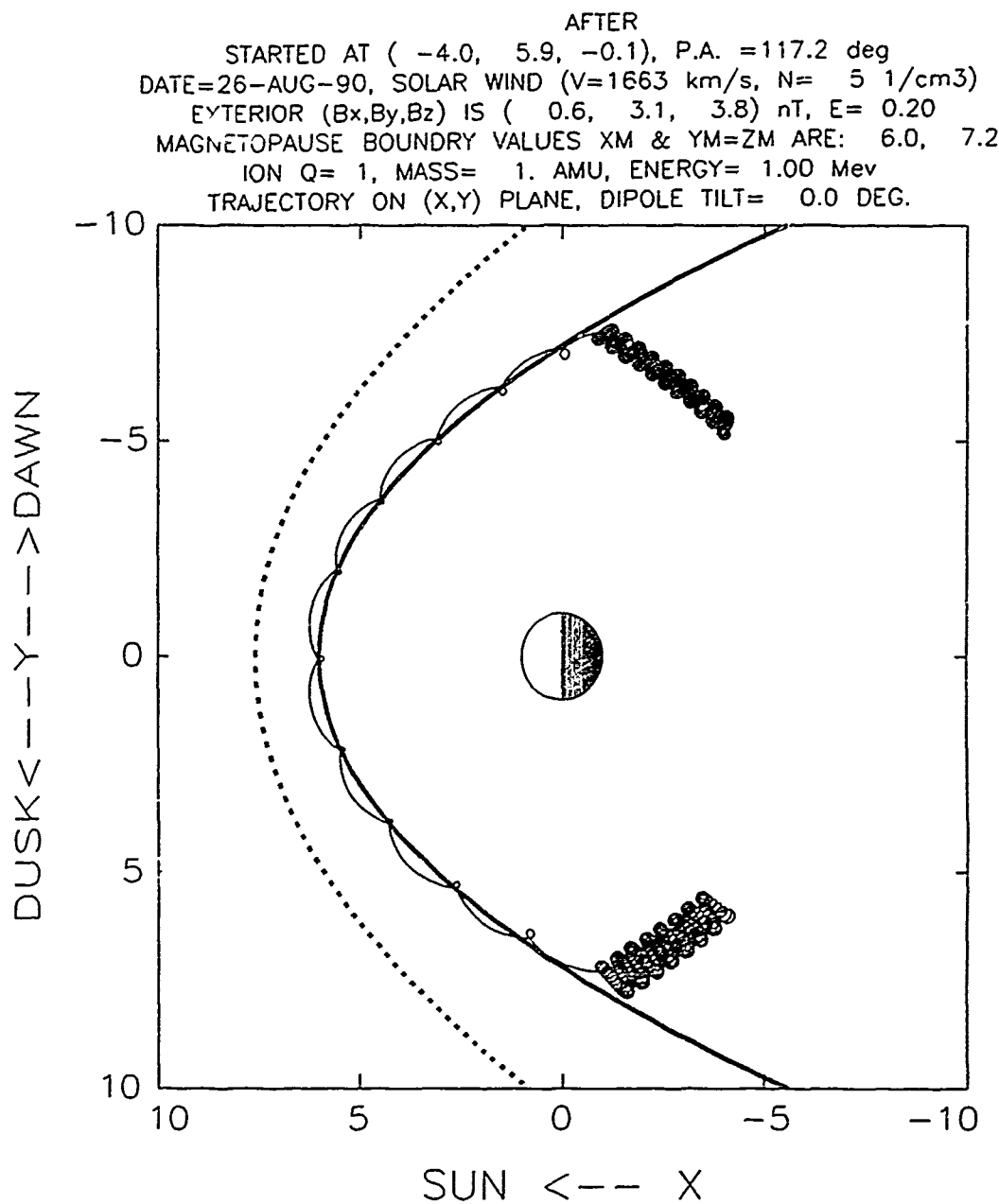


Figure 36

(DEPT. 91-20), LPARL PARTICLE TRAJECTORY CODE
 STARTED AT (-4.0, 5.9, -0.1), P.A. =117.2 deg
 DATE=11-FEB-91, SOLAR WIND (V=1663 km/s, N= 5 1/cm³)
 EXTERIOR (B_x,B_y,B_z) IS (0.6, 3.1, 3.8) nT, E= 0.20
 B_{ext}= 5.00*[1.+0.00*SIN(1.0*PHI+ 0.)+0.00*SIN(1.0*PHI+ 0.)]
 MAGNETOPAUSE BOUNDARY VALUES X_M & Y_M=Z_M ARE: 6.0, 7.2
 ION Q= 1, MASS= 1. AMU, ENERGY= 1.00 Mev
 TRAJECTORY ON (X,Z) PLANE, DIPOLE TILT= 0.0 DEG.

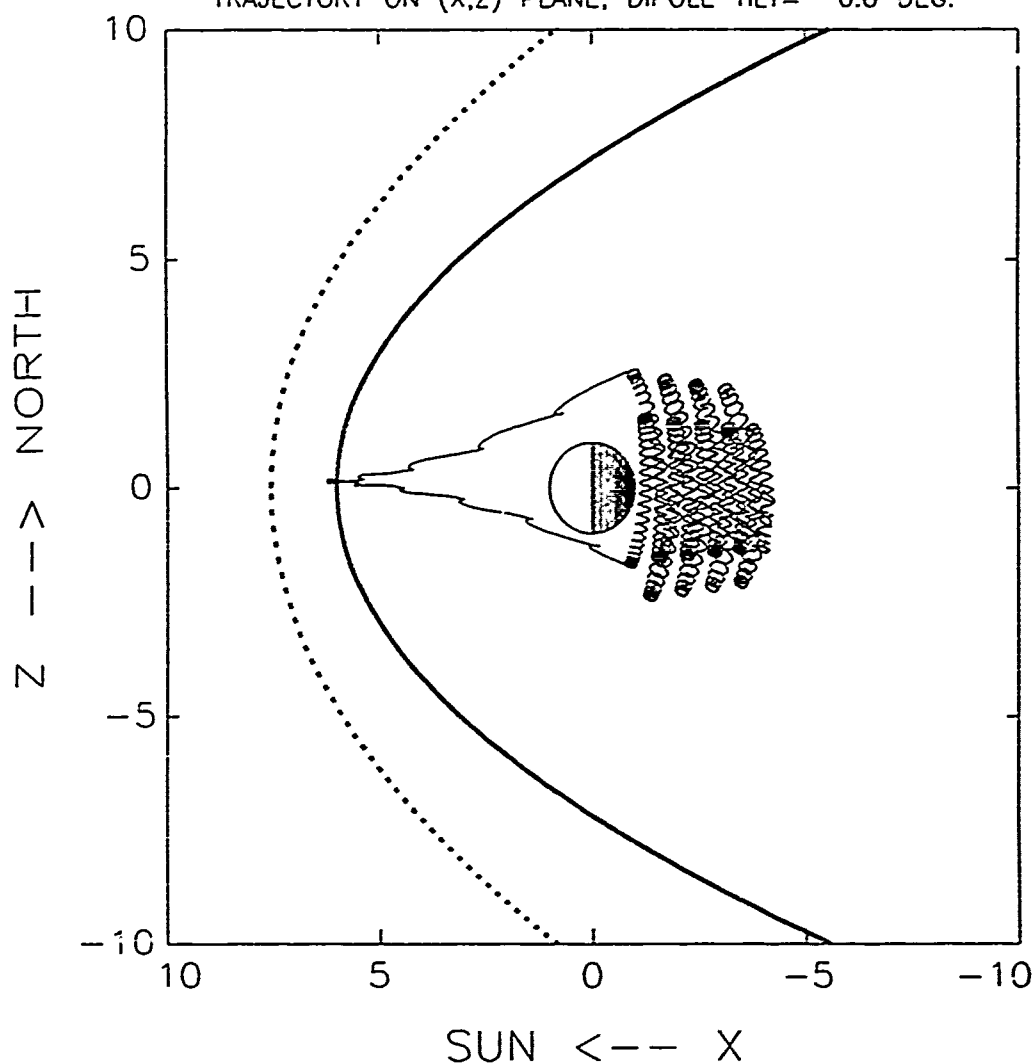


Figure 37

(DEPT. 91-20), LPARL PARTICLE TRAJECTORY CODE
 STARTED AT (-4.0, 5.9, -0.1), P.A. =117.2 deg
 DATE=11-FEB-91, SOLAR WIND (V=1663 km/s, N= 5 1/cm³)
 EXTERIOR (B_x,B_y,B_z) IS (0.6, 3.1, 3.8) nT, E= 0.20
 Bext= 5.00*[1.+0.00*SIN(1.0*PHI+ 0.)+0.00*SIN(1.0*PHI+ 0.)]
 MAGNETOPAUSE BOUNDARY VALUES XM & YM=ZM ARE: 6.0, 7.2
 ION Q= 1, MASS= 1. AMU, ENERGY= 1.00 Mev
 TRAJECTORY ON (Y,Z) PLANE, DIPOLE TILT= 0.0 DEG.

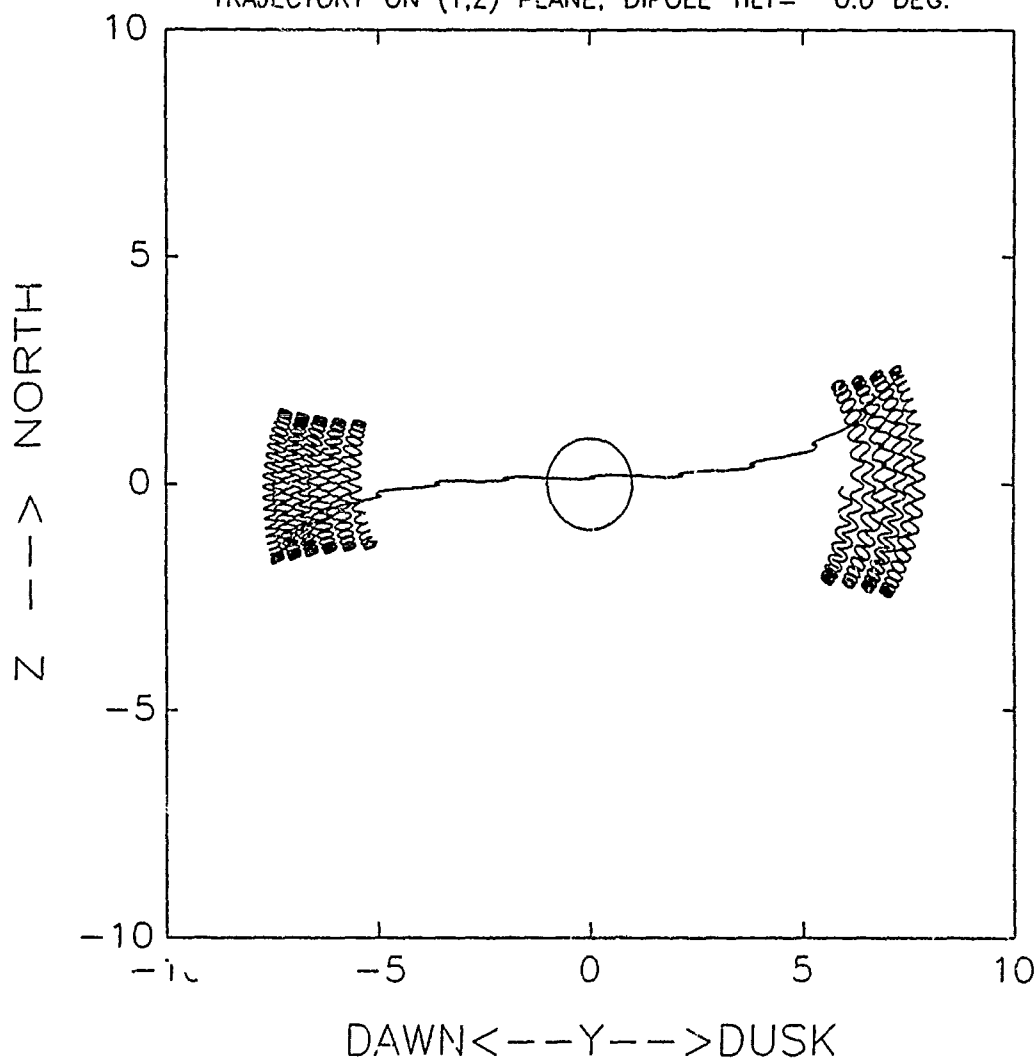


Figure 38

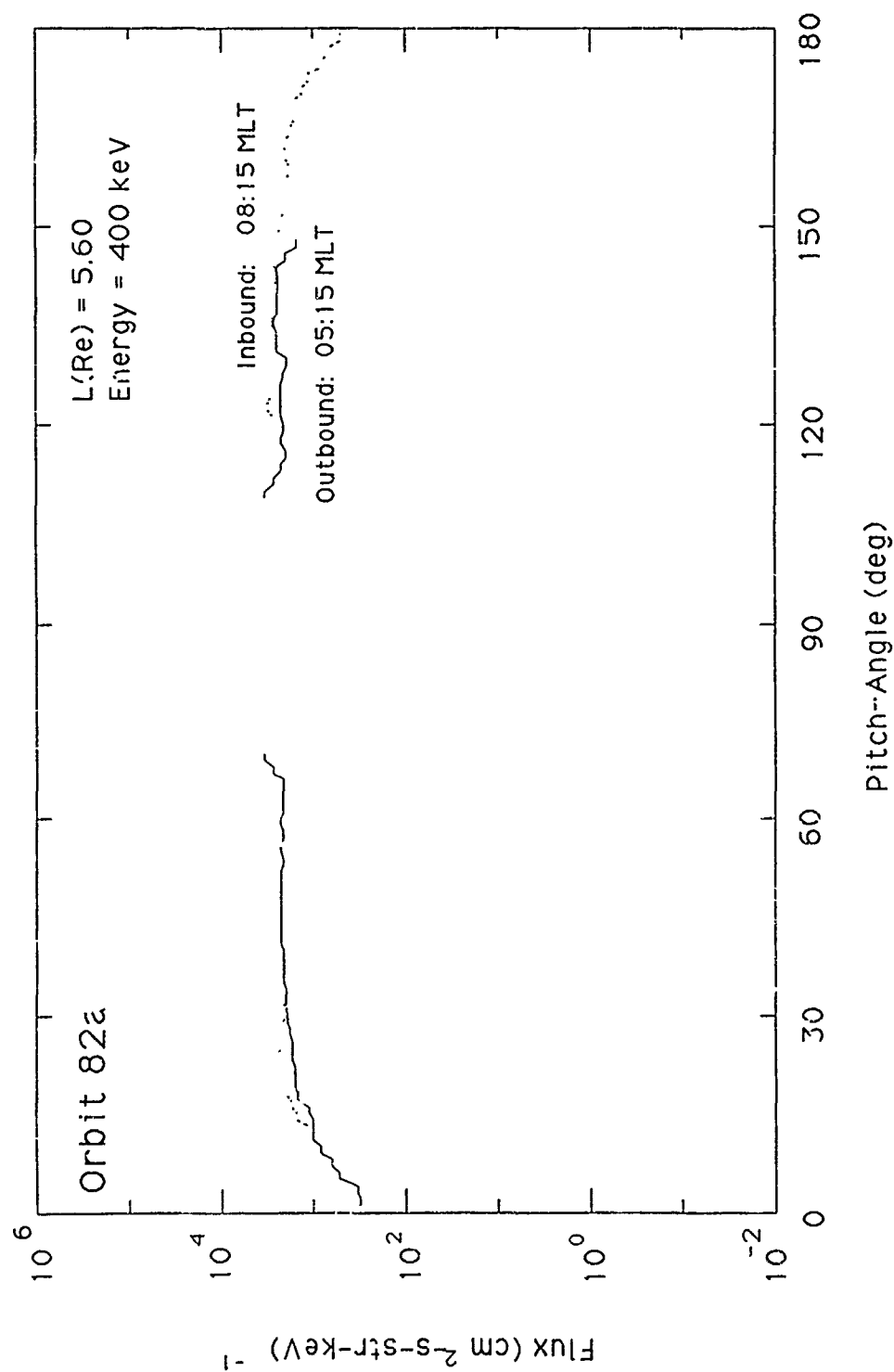


Figure 39

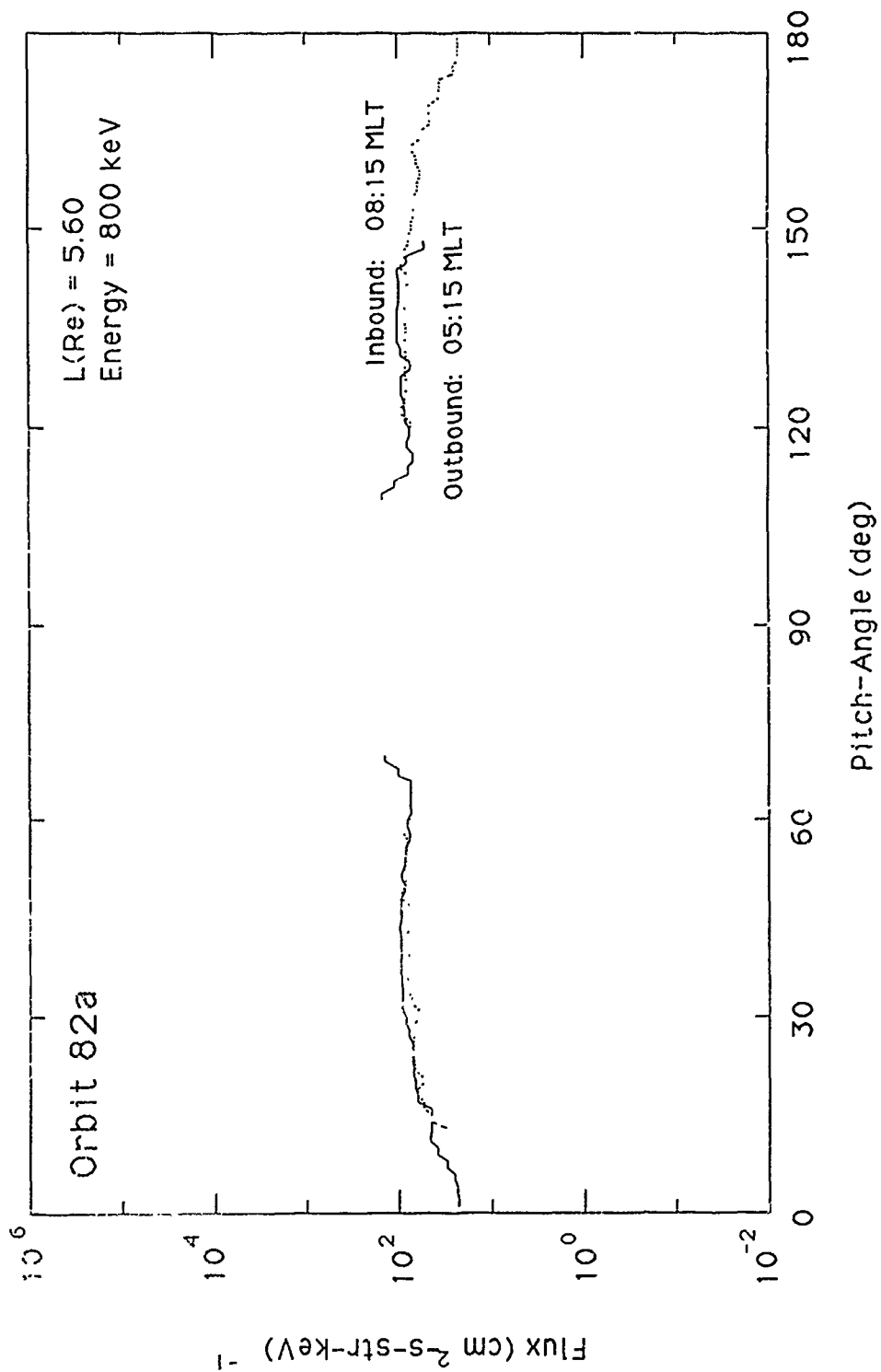


Figure 40